RESEARCH ARTICLE SUMMARY

ARCHAEOLOGY

Ancient lowland Maya complexity as revealed by airborne laser scanning of northern Guatemala

Marcello A. Canuto*†, Francisco Estrada-Belli*†, Thomas G. Garrison*†, Stephen D. Houston‡, Mary Jane Acuña, Milan Kováč, Damien Marken, Philippe Nondédéo, Luke Auld-Thomas‡, Cyril Castanet, David Chatelain, Carlos R. Chiriboga, Tomáš Drápela, Tibor Lieskovský, Alexandre Tokovinine, Antolín Velasquez, Juan C. Fernández-Díaz, Ramesh Shrestha

INTRODUCTION: Lowland Maya civilization flourished from 1000 BCE to 1500 CE in and around the Yucatan Peninsula. Known for its sophistication in writing, art, architecture, astronomy, and mathematics, this civilization is still obscured by inaccessible forest, and many questions remain about its makeup. In 2016, the Pacunam Lidar Initiative (PLI) undertook the largest lidar survey to date of the Maya region, mapping 2144 km^2 of the Maya Biosphere Reserve in Guatemala. The PLI data have made it possible to characterize ancient settlement and infrastructure over an extensive, varied, and representative swath of the central Maya Lowlands.

RATIONALE: Scholars first applied modern lidar technology to the lowland Maya area in 2009, focusing analysis on the immediate surroundings of individual sites. The PLI covers twice the area of any previous survey and involves a consortium of scholars conducting collaborative and complementary analyses of the entire survey region. This cooperation among scholars has provided a unique regional perspective revealing substantial ancient population as well as complex previously unrecognized landscape modifications at a grand scale throughout the central lowlands in the Yucatan peninsula.

RESULTS: Analysis identified 61,480 ancient structures in the survey region, resulting in a density of 29 structures/km^2. Controlling for a number of complex variables, we estimate an average density of ~80 to 120 persons/km^2 at the height of the Late Classic period (650 to 800 CE). Extrapolation of this settlement density to the entire 95,000 km^2 of the central lowlands produces a population range of 7 million to 11 million. Settlement distribution is not homogeneous, however; we found evidence of (i) rural areas with low overall density, (ii) periurban zones with small urban centers and dispersed populations, and (iii) urban zones where a single, large city integrated a wider population.

The PLI survey revealed a landscape heavily modified for intensive agriculture, necessary to sustain populations on this scale. Lidar shows field systems in the low-lying wetlands and terraces in the upland areas. The scale of wetland systems and their association with dense populations suggest centralized planning, whereas upland terraces cluster around residences, implying local management. Analysis identified 362 km^2 of deliberately modified agricultural terrain and another 952 km^2 of unmodified uplands for potential swidden use. Approximately 106 km of causeways within and between sites constitute evidence of inter- and intracommunity connectivity. In contrast, sizable defensive features point to societal disconnection and large-scale conflict.

ON OUR WEBSITE

Read the full article at http://dx.doi.org/10.1126/science.aau0137

CONCLUSION: The 2144 km^2 of lidar data acquired by the PLI alter interpretations of the ancient Maya at a regional scale. An ancient population in the millions was unevenly distributed across the central lowlands, with varying degrees of urbanization. Agricultural systems found in lidar indicate how these populations were supported, although an irregular distribution suggests the existence of a regional agricultural economy of great complexity. Substantial infrastructural investment in integrative features (causeways) and conflictive features (defensive systems) highlights the interconnectivity of the ancient lowland Maya landscape. These perspectives on the ancient Maya generate new questions, refine targets for fieldwork, elicit regional study across continuous landscapes, and advance Maya archaeology into a bold era of research and exploration. ■

The list of author affiliations is available in the full article online.
*Corresponding author. Email: mcanuto@tulane.edu (M.A.C.); festrad1@tulane.edu (F.E.-B.); tgarrison1@ithaca.edu (T.G.G.)
†These authors contributed equally to this work.
‡These authors contributed equally to this work.
Cite this article as M. A. Canuto *et al.*, *Science* **361**, eaau0137 (2018). DOI: 10.1126/science.aau0137

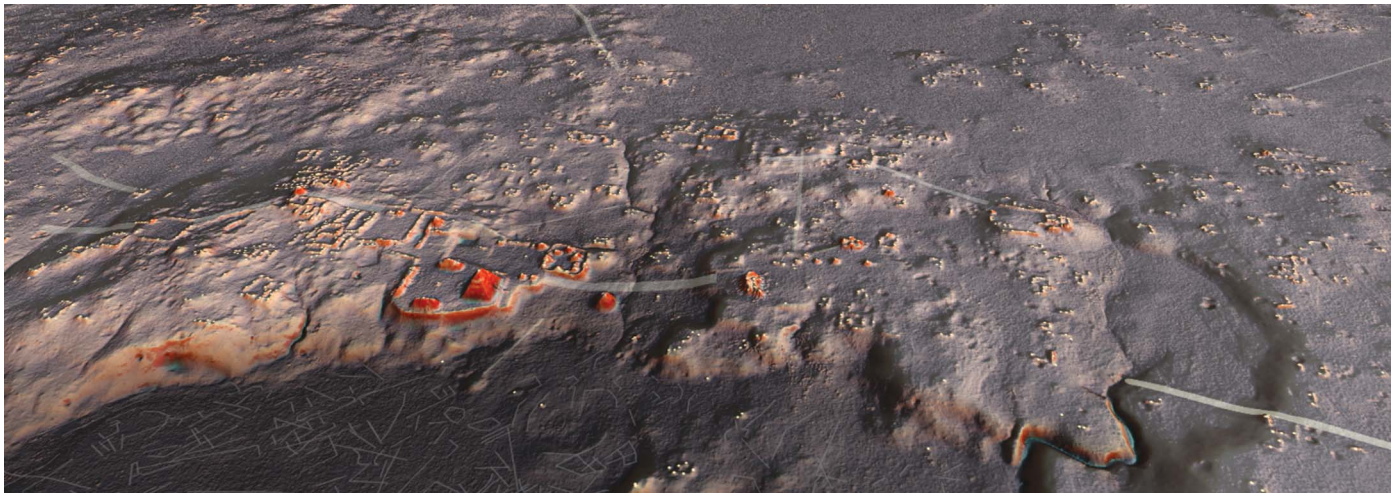

CREDIT: L. AULD-THOMAS AND M. A. CANUTO

Representation of the archaeological site of Naachtun, Petén, at twilight. Each ancient structure is marked by a yellow dot.

RESEARCH ARTICLE

ARCHAEOLOGY

Ancient lowland Maya complexity as revealed by airborne laser scanning of northern Guatemala

Marcello A. Canuto[1]*†, Francisco Estrada-Belli[1]*†, Thomas G. Garrison[2]*†, Stephen D. Houston[3]‡, Mary Jane Acuña[4], Milan Kováč[5], Damien Marken[6], Philippe Nondédéo[7], Luke Auld-Thomas[8]‡, Cyril Castanet[9], David Chatelain[8], Carlos R. Chiriboga[10], Tomáš Drápela[5], Tibor Lieskovský[11], Alexandre Tokovinine[12], Antolín Velasquez[13], Juan C. Fernández-Díaz[14], Ramesh Shrestha[14]

Lowland Maya civilization flourished in the tropical region of the Yucatan peninsula and environs for more than 2500 years (~1000 BCE to 1500 CE). Known for its sophistication in writing, art, architecture, astronomy, and mathematics, Maya civilization still poses questions about the nature of its cities and surrounding populations because of its location in an inaccessible forest. In 2016, an aerial lidar survey across 2144 square kilometers of northern Guatemala mapped natural terrain and archaeological features over several distinct areas. We present results from these data, revealing interconnected urban settlement and landscapes with extensive infrastructural development. Studied through a joint international effort of interdisciplinary teams sharing protocols, this lidar survey compels a reevaluation of Maya demography, agriculture, and political economy and suggests future avenues of field research.

Lowland Maya civilization flourished for nearly 2500 years (1000 BCE to 1500 CE) in southern Mexico, Guatemala, and Belize (Fig. 1), the central part of which consists of approximately 95,000 km^2 of rolling karst topography interspersed with wetlands (*1*). Today, this area is largely covered by tropical forest that has severely limited the scale of on-the-ground archaeological research, hindering regional assessments about ancient urbanism, population size, resource management, and sociopolitical complexity.

In 2016, the Pacunam Lidar Initiative (PLI) undertook the largest lidar survey to date of the lowland Maya region, mapping a total of 2144 km^2 of the Maya Biosphere Reserve (MBR) in Petén, Guatemala. This survey mapped 10 noncontiguous areas (polygons) ranging in size from 91 to 454 km^2, making it possible to characterize ancient settlement, agriculture, and physical infrastructure over an extensive and varied swath of the central Maya Lowlands by using a standardized and consistent dataset. Previous lidar surveys had taken place in Belize, Guatemala, and Mexico (*2*–*8*), providing important data on ancient lowland Maya civilization. However, the PLI sample, undertaken at far larger scale, captured greater variety in topography and ancient settlement for the central Maya Lowlands, the demographic and political heartland (*9*) of the Classic Maya culture. These data provide an opportunity to address current debates in Maya archaeology and to deepen studies of complex, tropical civilizations in the ancient world.

Some scholars suggest that the Maya Lowlands contained small city-state centers ruled by warring elites (*10*–*13*), in settlements supported by a relatively sparse rural population practicing swidden farming (*14*), with only limited input from intensive agriculture (*15*–*21*). In contrast, other views point to a regional network of densely populated cities with complex integrative mechanisms (*22*–*25*) that depended on heavy labor investments inside and outside urban cores (*15*, *26*, *27*). Even though the latter view has been ascendant in recent years, the absence of regional data has left the debate unresolved. The PLI data cover a sufficiently large area to provide robust support for the latter model and offer further insights about human-environment interactions in the region, including unexpectedly extensive fortifications and road networks.

Data collection, processing, and field validation

Lidar is an active remote sensing technology that uses laser pulses to map landcover and ground surface in three-dimensional space. The PLI effort collected lidar data with a Teledyne Optech Titan MultiWave multichannel, multispectral, narrow–pulse width lidar system, the most advanced aerial lidar system (*28*) deployed in the region to date (Table 1). The improvements include scanning of the terrain from six different view angles (versus the more usual two views) and higher sensor-range resolution, enabling more precise mapping of topographic signatures under short vegetation. The data collection was designed with a nominal laser density of 15 pulses/m^2 from a flying altitude of 650 m above ground level. The fidelity of this sensor reveals details of local topography, ancient architectural and agricultural features, and damage from looting (Fig. 2).

The data were collected in 10 polygons over 12 designated survey blocks (Table 1). Each survey block was named for the largest known archaeological site within its boundaries; two survey blocks in archaeologically unknown areas were designated Env 1 and Env 2. The current dataset arose from roughly 33.5 billion laser pulses, producing about 60 billion returns, of which 5.2 billion were classified as ground returns. The average ground densities for different polygons range from 1.1 to 5.3 returns/m^2, the result of varying vegetation densities and canopy coverage across the survey area. Of the total mapped area, 23% has an average ground return density of 1.1 returns/m^2, 60% has a ground return density range of 1.5 to 2.7 returns/m^2, and 17% has an average ground return density of more than 5.2 returns/m^2. These data were interpolated to create bare-earth terrain models with a spatial resolution of 1 m per grid cell.

Identification of archaeological features within the lidar dataset was iterative (*29*). The PLI study region has been subject to thousands of person-days of pedestrian survey over the course of eight decades of field research. Consequently, there was an extensive "ground-truthed" dataset available for most survey blocks (Fig. 3). Analysts from each participating team made preliminary identifications using existing site maps as training samples. Features of archaeological interest were identified through visual inspection of lidar-derived terrain models. Multiple visualization rasters and manual identification were used to highlight distinct kinds of topographic features (Fig. 4); Table 2 specifies the range of greatest utility in such visualizations. In addition to previously published methods (*30*–*32*), we developed a new technique, "prismatic openness" (*33*), that

[1]Middle American Research Institute, Tulane University, New Orleans, LA, USA. [2]Department of Anthropology, Ithaca College, Ithaca, NY, USA. [3]Department of Anthropology, Brown University, Providence, RI, USA. [4]Department of Anthropology, Washington University, St. Louis, MO, USA. [5]Center for Mesoamerican Studies, Comenius University, Bratislava, Slovakia. [6]Department of Anthropology, Bloomsburg University, Bloomsburg, PA, USA. [7]CNRS–ARCHAM UMR 8096, Université Paris 1–Panthéon-Sorbonne, Paris, France. [8]Department of Anthropology, Tulane University, New Orleans, LA, USA. [9]Laboratoire de Géographie Physique–CNRS UMR 8591, Université Paris 8, Paris, France. [10]Department of Anthropology, Yale University, New Haven, CT, USA. [11]Department of Theoretical Geodesy, Slovak University of Technology, Bratislava, Slovakia. [12]Department of Anthropology, University of Alabama, Tuscaloosa, AL, USA. [13]Universidad de San Carlos de Guatemala, Guatemala City, Guatemala. [14]National Center for Airborne Laser Mapping, University of Houston, Houston, TX, USA.
***Corresponding author. Email: mcanuto@tulane.edu (M.A.C.); festrad1@tulane.edu (F.E.-B.); tgarrison1@ithaca.edu (T.G.G.)** †These authors contributed equally to this work. ‡These authors contributed equally to this work.

facilitated detection of small features such as simple house platforms and agricultural terraces.

After preliminary identifications backed by preexisting map and excavation data, ground-truthing and test excavations occurred in 2017 within the Holmul, Corona, Perú, Naachtun, Tintal, Uaxactun, and Zotz survey blocks. This allowed each project to (i) calibrate their feature identifications to ground conditions and (ii) identify patterns in false-positive and false-negative identifications. With this knowledge in hand, a second wave of feature identification took place from August to December 2017.

Overall, approximately 165 km^2 within the study area have either been used as training samples, subsequently "ground-truthed," or both (Table 3); that is, 7.7% of the entire PLI survey region has been verified through ground survey, although mapped areas were not uniformly distributed (Table 3). Moreover, all field teams within the PLI study region have ground-validated features belonging to every class reported on here: buildings of various types, defensive features, upland and wetland agricultural features, causeways, canals, and reservoirs.

PLI's preliminary field validation efforts suggest that the feature identifications are accurate if slightly conservative. Most projects report a net increase in field-verified structures of ~15% over those identified through visual analysis of the lidar data. Furthermore, certain features—in particular, small channels or berms as well as large causeways—are clearly visible in the lidar although almost impossible to recognize on the ground without excavation, meaning that in-field visual inspection alone is not always capable of assessing the accuracy of lidar feature identifications. Nonetheless, because ground-truthing efforts are ongoing, and because error rates (false positives and negatives) are likely to vary for different classes of features, all analyses presented here use the 2017 PLI feature dataset with no further adjustments.

Population estimates

Using the above methodology, 61,480 structures have been identified in the PLI survey region, resulting in an aggregate settlement density of 29 structures/km^2 (Table 4). Because this structure count derives from a much-expanded and regionally representative dataset, it can serve as the basis for a uniquely robust regional population estimate. Even so, producing population estimates from archaeological data requires some assumptions of varying detail and scope from ethnographic analogy and archaeological data; as a consequence, the exercise comes with some degree of uncertainty that only future field research can reduce.

To estimate Late Classic population from structure counts, well-established methodologies for the Maya Lowlands were adjusted by controlling for invisible structures, contemporaneity of use, nonresidential function, non–Late Classic occupation, and numbers of individuals per building (Table 5) (*34*). The values of these adjustments vary widely across the literature, given the regional variability of the archaeological record. The geographic scope of the PLI study area, which includes diverse landscapes with distinct settlement histories, necessitates a broader view beyond any single set of local adjustments. As such, values for each adjustment were collated from published scholarship and categorized into five sets according to their overall impact (minimum, low, middle, high, and maximum). All adjustments were then multiplied to derive a composite population index range (*PopIndex*), which, when multiplied by the total number of structures, produced an overall population range (*29*).

Population estimates were calculated to the nearest half million to avoid false precision and are presented as a range rather than a single value for the central Maya Lowlands. Given the nature of the available excavation data, this study does not propose a diachronic demographic curve. It only estimates total population during the Late Classic population maximum, 650 to 800 CE, because all PLI survey blocks subjected to archaeological investigation have shown evidence for substantial Late Classic populations.

Following this procedure and guidelines, we estimate a Late Classic population range of 150,000 to 240,000 for the entire PLI survey region. This number amounts to an average density of ~80 to 120 persons/km^2. This density value accords with the ~100 persons/km^2 suggested by previous nonlidar research (*9*, *34*–*37*). Inomata *et al.*'s recently published lidar-derived settlement data from the Ceibal region (with

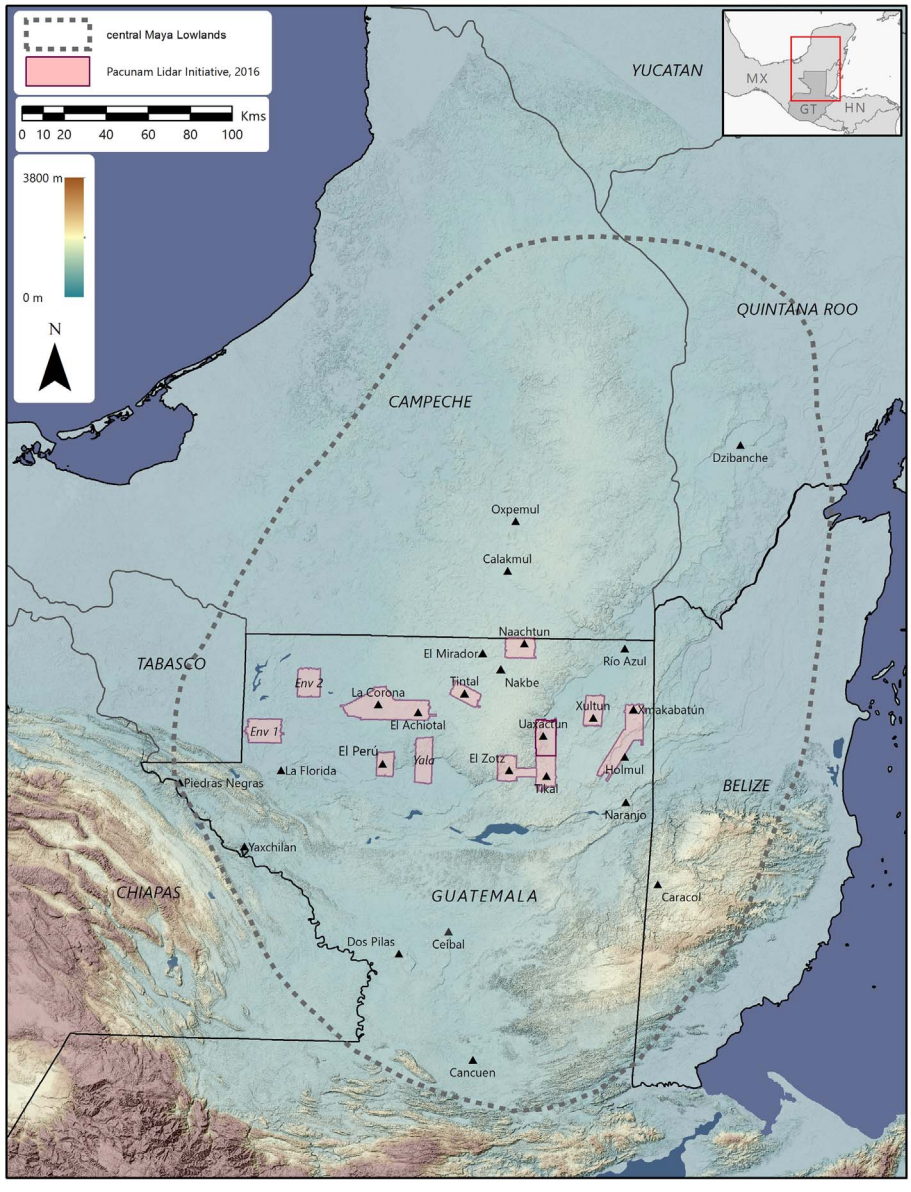

Fig. 1. Distribution of 12 PLI survey blocks. Location of 12 PLI survey blocks in relation to the central Maya Lowlands area as well as to the sites mentioned in text; for those survey blocks without a named site, the name of the block is provided (i.e., Env 1, Env 2, and Yala).

Table 1. Lidar ground point averages. Important archaeological sites and lidar ground point densities within each PLI polygon.

Polygon	Survey block	Main archaeological site(s)	Area (km^2)	Lidar returns: Total points	Lidar returns: Ground points	Ground points/m^2
1601	Holmul	Holmul	308.64	8,294,456,212	310,174,174	1.11
		Xmakabatun				
1602	Xultun	Xultun	124.02	3,427,027,990	138,067,383	1.13
		San Bartolo				
1603	Tikal	Tikal	146.93	14,614,355,752	926,848,573	2.07
	Uaxactun	Uaxactun	163			
	Zotz	El Zotz	143.73			
1604	Naachtun	Naachtun	135.29	3,666,496,941	197,825,181	1.48
1605	Tintal	Tintal	97.05	3,118,138,624	184,909,324	1.94
1606	Corona	La Corona	431.67	12,388,384,352	1,144,897,043	2.72
		El Achiotal				
1607	Yala	—	172.27	4,495,443,060	331,572,441	1.95
1608	Perú	El Perú-Waka'	91.27	2,302,198,440	97,224,397	1.09
1609	Env 2	—	145.66	3,599,229,811	868,902,279	5.17
1610	Env 1	—	184.28	4,147,724,212	971,717,525	5.32
		Total	2,143.81	60,053,455,394	5,172,138,320	2.45

Fig. 2. Close-up of Xmakabatun. Image of Xmakabatun that demonstrates the high-fidelity detail of the Teledyne Opech Titan sensor. (**A**) Looting depressions highlighted by an openness visualization. (**B**) Looting features as drawn in the field (shown in red) as well as evidence of monumental architecture, causeways, residential structures, ditches, and terraces.

31 observed structures/km^2 across a sample of 470 km^2) (*38*) are consistent with the settlement data presented here.

There is substantial variability in settlement density across the PLI survey blocks, which reflects a pattern characteristic of the entire central Maya Lowlands. That is, some areas will be densely settled (comparable to the Tikal, Xultun, or Naachtun survey blocks) and others will be sparsely occupied (comparable to the Corona, Yala, and Env 1 and 2 survey blocks). However, because average settlement density over large areas is likely to be similar, the PLI dataset can be extrapolated with confidence over a 95,000-km^2 area known as the "central Maya Lowlands" (Fig. 1). This area excludes the northern Yucatan, the Gulf Coast plains, and coastal Belize and Quintana Roo because they differ physiogeographically from the PLI survey region.

The Late Classic population for the central Maya Lowlands was calculated by multiplying (i) the mean structure density (structures per km^2) of the sample, (ii) the total area of the central Maya Lowlands (95,000 km^2), and (iii) the *PopIndex* range (see below):

$$\text{Population} = \frac{\text{Total number of structures}}{\text{Total area surveyed}} \times 95,000 \times \textit{PopIndex} \quad (1)$$

This formula suggests that 61,480 identified structures within 2144 km^2 of PLI's surveyed area can be extrapolated to 2,724,396 structures over an area of 95,000 km^2. Once multiplied by the *PopIndex* range, these numbers yield a population range of 7 million to 11 million for the central Maya Lowlands during the Late Classic period. Notably, this range aligns with the upper end of prior estimates for the same region, derived from pedestrian surveys (*36*, *39*–*41*). The incorporation of Inomata *et al.*'s published data from Ceibal (*38*) to both PLI's structure and coverage area totals results in the same extrapolated population levels for the central Maya Lowlands—a good indication that the PLI dataset is a representative sample for the region and that the extrapolations are sound.

This estimate is moderate, even conservative, primarily for two reasons: (i) The traditional method of calculating regional population—multiplying area (95,000 km^2) by a constant population density (80 to 120 persons/km^2)—has been found to underestimate the resident populations of larger centers (Tikal, Naachtun)

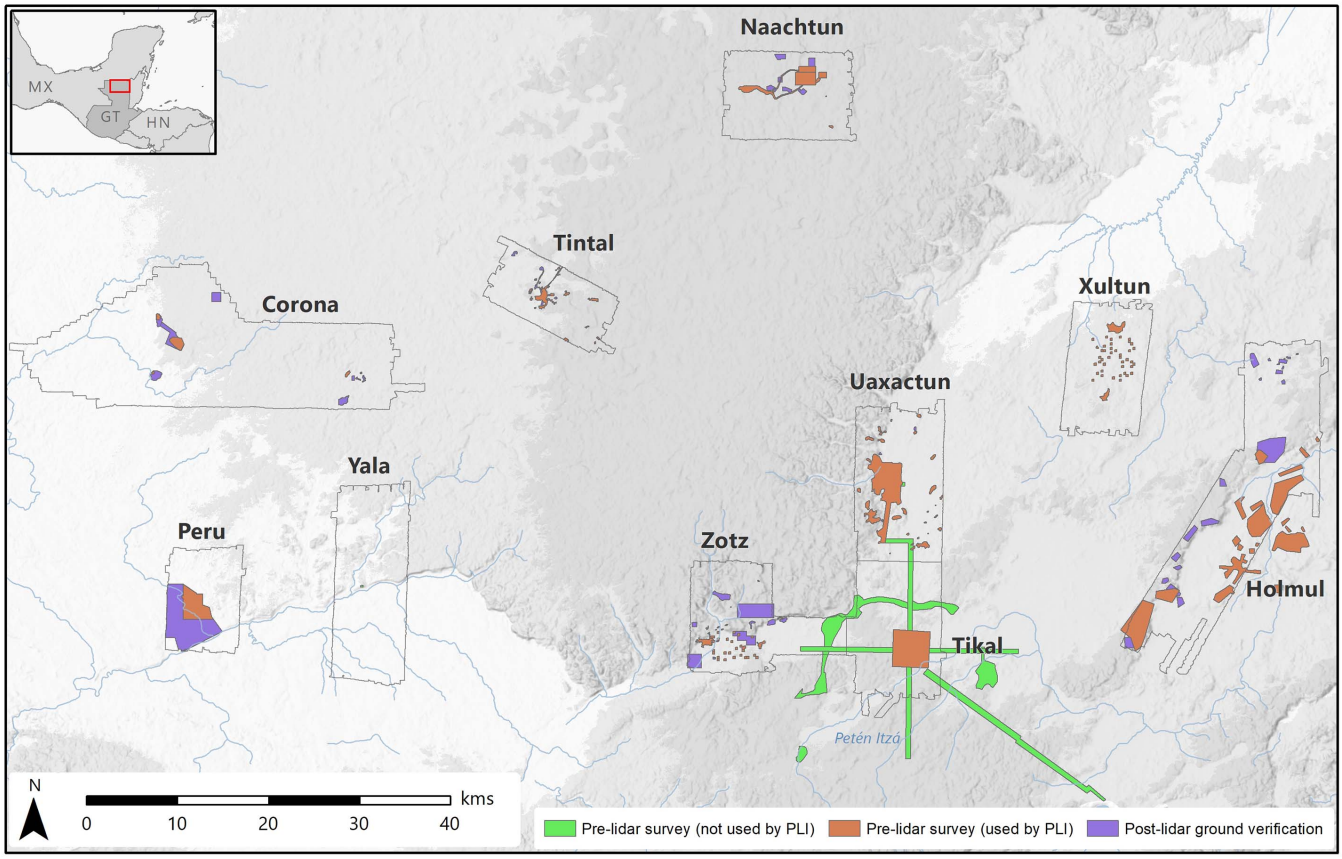

Fig. 3. Mapped areas within PLI zone. Map of survey blocks showing (i) areas covered by pedestrian surveys before acquisition of lidar data and (ii) areas where ground verification of the lidar data has been completed to date.

Table 2. Lidar visualizations. Raster visualization combinations created and used for feature identifications.

Terrain visualization	Raster combo	Color ramp/band combo	Transparency	Utility	Notes
Simple Local Relief Model (SLRM)				Very small buildings, slight depressions, agricultural features	
Layer 1	SLRM	Black to white	0%		Created in Relief Visualization Toolbox (RVT) (*30*)
Modified Red Relief Image Map (RRIM)				Small buildings, depressions, contour terraces	Based on procedures detailed in (*31*)
Layer 1	Slope	Custom: white to red	0%		Created in ArcToolbox Slope; visualized in QGIS with blending mode "multiply"
Layer 2	SLRM	Custom: blue-gray-yellow	0%		Created in RVT (*30*)
Sky-View Factor (SVF)				Depressions, orthogonal buildings	
Layer 1	SVF	Black to white	0%		Created in RVT (*30*, *32*)
Prismatic Openness				Small buildings, agricultural features	"Openness" (*33*)
Layer 1	Positive openness	White to black	50%		Created in RVT (*30*)
Layer 2	Negative openness	Black to white	50%		Created in RVT (*30*)
Layer 3	16-dir. hillshade	RGB: 3,2,1	0%		Created in RVT (*30*) with vertical exaggeration of 3–5

that become denser with increasing scale (42). Accordingly, the densest urban areas likely would have contained more people than these current approximations. (ii) Although comparison of lidar-derived structure data and pedestrian survey data shows strong agreement within the PLI survey area, vegetation and taphonomic factors reduce the visibility of small structures in lidar-based visualizations. Ground validation of the PLI lidar-derived dataset has resulted in a ~15% net increase in archaeological structures. Because both of these factors would result in larger populations, only further fieldwork can render these estimates more accurate.

Regardless of these caveats, the PLI data suggest overall regional populations of such scale that some degree of agricultural intensification (43–45) would have been required to sustain them. Approximately half of the central Lowlands are seasonal wetlands known as *bajos* (15). Because permanent settlements tended to avoid these flood-prone and poorly drained areas, they remained largely uninhabited and could then be available, after added investment, to intensive agriculture (46).

Table 3. Extent mapping and ground verification. Areas in the PLI survey region covered by both pre-lidar pedestrian surveys and post-lidar ground validation efforts (these sometimes overlap).

Site	Area (km²)	Pre-lidar pedestrian survey (km²)	Used by PLI		
			Pre-lidar pedestrian survey (km²)	Post-lidar ground validation (km²)	Combined sampled area (km²)
Corona	432	2.0	2.0	6.9	6.9
Env 1	184	0.0	0.0	0.0	0.0
Env 2	146	0.0	0.0	0.0	0.0
Holmul	309	46.0	37.0	16.3	50.8
Naachtun	135	7.9	7.9	7.7	15.6
Perú	91	8.2	8.2	21.6	29.8
Tikal	147	86.2	16.3	0.0	16.3
Tintal	97	2.8	2.8	1.0	3.8
Uaxactun	163	21.4	21.4	0.5	21.9
Xultun	124	4.6	4.6	0.0	4.6
Yala	172	0.04	0.0	0.0	0.0
Zotz	144	3.1	3.1	16.0	16.0
Total	2144	182.2	103.2	70.0	165.6

Table 4. Total structures and settlement density estimates by PLI survey blocks.

Name	Area (km²)	Structures	Structures/km²
Corona	432	3,629	8
Env 1	184	307	2
Env 2	146	254	2
Holmul	309	7,207	23
Naachtun	135	11,979	89
Perú	91	4,096	45
Tikal	147	12,341	84
Tintal	97	4,130	43
Uaxactun	163	5,075	31
Xultun	124	5,513	44
Yala	172	740	4
Zotz	144	6,254	44
Total	2,144	61,480	29

Table 5. *PopIndex* calculations. Set of adjustments used to calculate a "population index" (*PopIndex*), which produces an estimated population when multiplied by structure number. The range in the value of each adjustment indicates the variation within the published record.

Adjustment	Min	Low	Middle	High	Max
1. Invisible or hidden structures	110%	110%	110%	110%	110%
2. Contemporaneity of occupation	75%	80%	83%	87%	90%
3. Residential structures	75%	80%	81.1%	83.5%	85.7%
4. Late Classic	80%	83%	87.5%	92%	95%
5. Persons per structure	4.00	4.37	4.89	5.40	5.60
PopIndex (for Late Classic)	1.98	2.55	3.16	3.97	4.51

Agricultural intensification

Early applications of airborne synthetic aperture radar (SAR) suggested the existence of wetland field systems throughout the entire central Maya Lowlands (47–49). However, most of the patterns identified as evidence of intensive agricultural features were later dismissed as "noise" in the imagery or artifacts of the local geology (15, 21, 50–52). Furthermore, given that most of the wetlands in the interior of the peninsula contain clay vertisols, their overall suitability for ancient agriculture was challenged (17, 50, 52–57). Although aerial photography and fieldwork succeeded in identifying both upland and wetland intensive agricultural features in various zones within the lowlands (58–60), the extent of known agricultural improvements remained limited to a few specific areas (18–20, 55, 61–67).

Even though the idea that lowland Maya society only relied on swidden was discarded in the 1980s in favor of a "new orthodoxy" claiming some reliance on a mosaic of more intensive agricultural strategies, the dominant view among specialists was that wetland agriculture was generally limited to areas peripheral to the central Maya Lowlands and that the elevated interior would have relied primarily on swidden agriculture (15, 18, 19, 27, 50, 52, 54, 61–63, 68, 69).

The PLI survey revealed a landscape heavily modified for intensive agriculture: 11 of the 12 survey blocks include agricultural features of some kind. In wetland areas, the survey primarily identified drainage channels. These were designed either to draw water away from natural streams toward infrequently flooded areas or to drain those same areas during major floods. Their dimensions vary from 1 to 2 m in width and 20 to 50 cm in depth. Major channels can measure more than 1 km in length (one extreme case at Tintal is 2.5 km long). Large and small channels intersected at regular intervals, forming nested grids within "channelized" fields (Fig. 5). Overall, these data suggest that wetlands throughout the central Maya Lowlands were modified for agricultural exploitation (16, 43, 61, 62, 70), rather than being used exclusively as sources of water and transportable soils (16, 71). The largest total area of wetland

agriculture is found in the Naachtun region, with 31.5 km^2 of interspersed channelized zones, followed by Holmul and Tikal. The largest single zones of contiguous wetland fields occur in the Holmul survey block, ranging from 2.3 to 7 km^2, followed by Tikal and Naachtun. These wetlands may have been selected because of local edaphic conditions, yet they also lie near the most populated areas.

On upland terrain, numerous linear stone features such as terraces and low field walls were identified. These features measure 1 to 2 m in width and are no higher than 50 cm. Some are strictly linear (i.e., contour terraces and check dams); others create enclosures (Fig. 5). Several features form gridded fields with or without enclosure walls, and, in some examples, surround residential structures similar to the *albarradas* (circular walls) of the northern Maya Lowlands (*72*). Because of their multiple functions, stone features vary widely in length, from only a few meters to >1 km.

By identifying these features, we defined "zones of intensive cultivation" (*29*) where agricultural improvements were either the only feature in the landscape (e.g., wetland fields) or were interspersed with settlement. The latter case encompasses production systems generally described as infields, orchards, and houselot gardens. A total of 67 km^2 (6659 ha) of wetland fields and 295 km^2 (29,517 ha) of upland fields were classified as zones of intensive cultivation, accounting for ~17% (362 km^2) of the entire PLI survey area. Investments in upland agriculture are most common in the central and eastern sectors of our sample. The largest area totals occur, by descending order, in the Tikal (64 km^2), Uaxactun (57 km^2), Naachtun (47 km^2), and Xultun (45 km^2) survey blocks.

Estimates for the overall productive capacity of this heavily modified agricultural landscape were calculated to determine whether it could have supported the Late Classic populations reported above. Little ethnographic information on the productivity of intensive agriculture in the Maya Lowlands is available, so estimations of overall productive capacity must rely on the productivity of swidden agriculture as the sole point of reference. Because some of the improved agricultural land was unusable (e.g., *bajo*) or prone to rapid degradation (e.g., erosible slopes), many improvements would have succeeded in extending productivity to otherwise unproductive areas (*73*). However, because some upland features were indeed placed on optimal land (i.e., gentle slopes) and the moisture-retaining properties of terraces improve agricultural productivity (*37*, *74*), it is likely that some upland features did improve overall yields beyond what traditional swidden agriculture could produce. Nonetheless, these calculations assume that all zones of intensive cultivation resulted in the same productive capacity as swidden.

Ethnographic data on the productivity of traditional lowland Maya swidden agriculture were collated and standardized to estimate the number of hectares necessary to support one person. Data on swidden productivity were drawn from Cowgill (*75*–*77*), Griffin (*78*), Schwartz (*79*, *80*), Nations and Nigh (*81*), and Ford and Nigh (*37*). Standardization entailed, among other adjustments, normalizing the annual productivity of different fallow regimes to multiyear averages. These calculations resulted in a mean productivity value of 0.48 ha per person [the mean of the range (0.34 to 0.62 ha per person) resulting from using different adjustments from the above-cited sources] (table S3). This value was then applied to all the land in the PLI sample (1314 km^2) available for agricultural production (zones of intensive cultivation and nonwetland rural areas) to derive a maximum supportable population. Finally, by the same logic applied to population estimates, this number was adjusted to account for the possibility that these features of agricultural intensification were not all coeval. These calculations (Table 6) suggest that the total amount of land available for agricultural production in the PLI sample would have been more than sufficient to sustain the population levels reported above (*29*).

Consequently, the PLI data indicate some combination of the following possibilities: (i) There was capacity for surplus food production; (ii) substantial portions of agricultural land

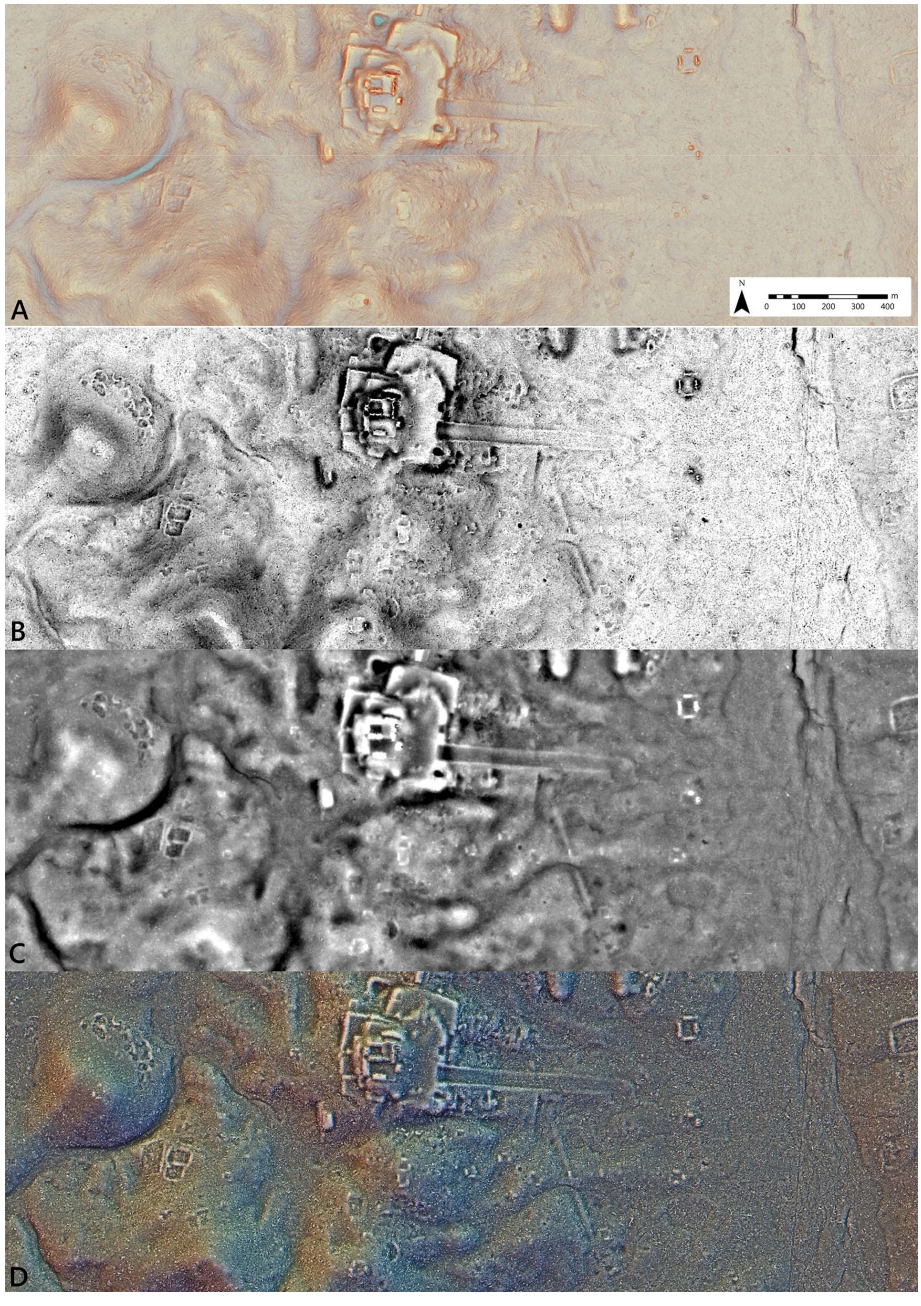

Fig. 4. Visualizations used for lidar analysis. (**A**) Red Relief Image Map (RRIM); (**B**) Sky-View Factor (SVF); (**C**) Simple Local Relief Model (SLRM); (**D**) Prismatic Openness.

were dedicated to the production of nonfoodstuffs (such as cotton or cacao); (iii) large areas of the uplands remained covered in forest (*37*, *82*, *83*); or (iv) populations were higher than our current estimates. Agricultural intensification could also have been achieved using strategies such as fallow-period shortening, multicropping, and manipulation of crop sociology; these would not have occasioned changes to the landscape visible in lidar. In addition to corn, a variety of other edible plants and fruit trees are known to have been grown in and around improved upland fields (*14*). Therefore, this study's reliance on both physical infrastructure (as an index for intensification) and ethnographic data of modern swidden productivity likely underestimates the total productive capacity of ancient lowland Maya agriculture.

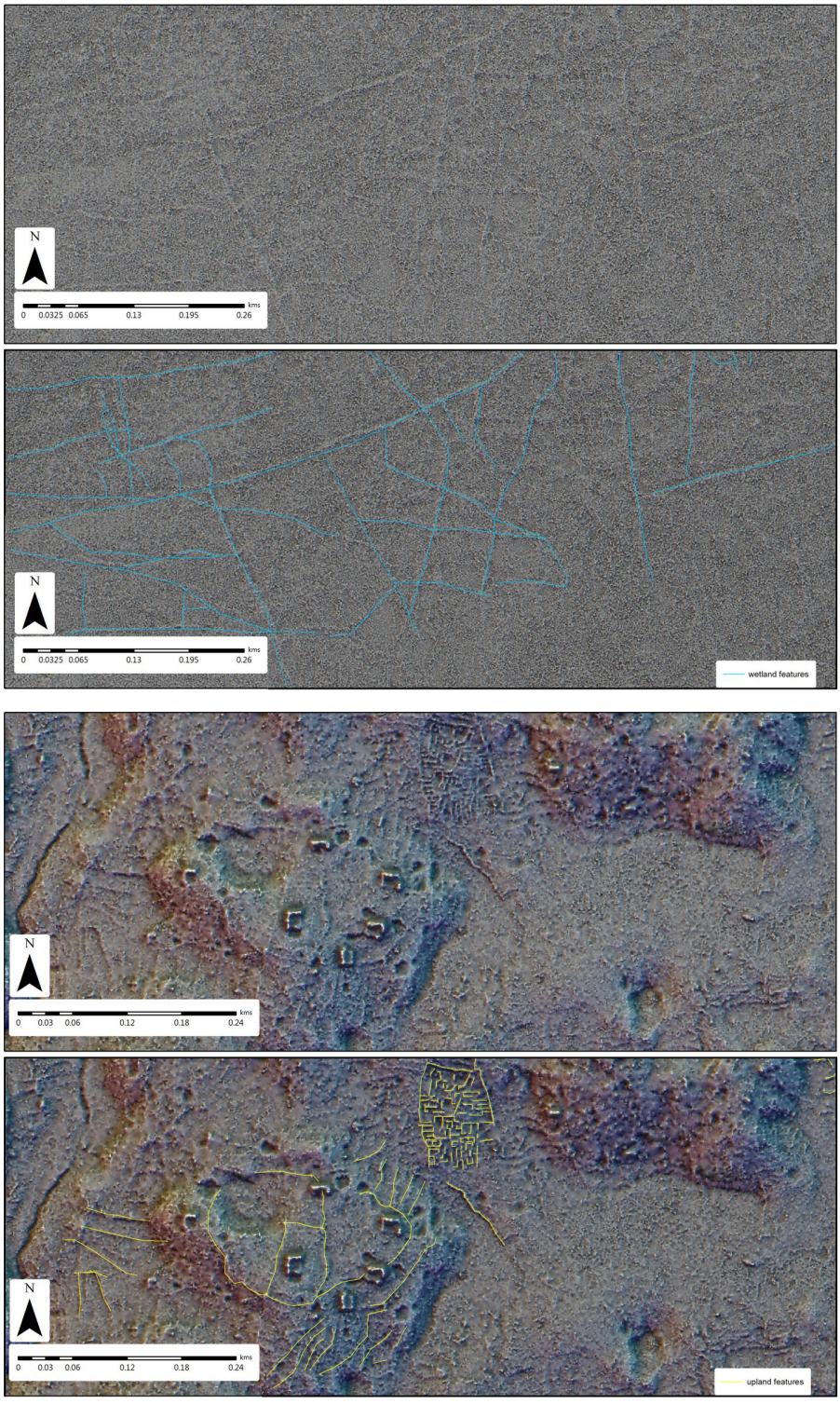

Fig. 5. Wetland and upland agricultural features. Examples of intensive wetland fields featuring networks of canals (above) and upland field zones featuring low stone wall features and terraces.

This dataset also demonstrates great variability in agricultural investment across the region (Fig. 6). The Corona survey block (432 km^2) has <1% of its available land improved for cultivation, whereas the Tikal block (147 km^2) has as much as 70%. Indeed, the lowest densities of agricultural features occur in the less populated western blocks of the sample, and the highest densities are located in the central and eastern sectors where settlement is densest. Across the PLI sample, areas defined here as periurban and urban (see below) contained the greatest relative density of agricultural features. Urban cores contained no agricultural features, whereas rural areas contained relatively fewer improved fields (Table 7 and Fig. 6). The scale of wetland field systems and their close association with densely populated areas suggest some degree of centralized involvement. Conversely, agricultural modifications of the uplands cluster around residential groups, which suggests that they were likely managed by household or small corporate groups. Upland improvements and terracing are common, likely making a substantial contribution to overall regional production (*26*).

The co-occurrence of dense settlement with agricultural improvements suggests that investments to maximize agricultural production were directed to areas where population sprawl limited the possibility for extensive farming. Despite these efforts, however, the estimated yield of the agricultural lands within the most heavily modified survey blocks—Tikal, Naachtun, Xultun, and Perú—would not have been sufficient to sustain their populations (Table 6). Even if the zones of intensive cultivation within these survey blocks had been twice as productive as swidden fields, none of these areas would have harvested enough to achieve self-sufficiency. That is, people living in these blocks were partly dependent on foodstuffs imported from surrounding areas. Such data point to a lowland Maya landscape that was a mosaic of interdependent densely populated political centers and extensive periurban hinterlands engaged in a complex set of interactions.

Urbanization

Settlement studies at lowland Maya sites have often used categories such as "site core," "periphery," and "rural" to delimit zones of different settlement density (*84*–*86*). These are useful categories at local scales. However, the scope of the PLI dataset allowed for a comparison of settlement density at a regional level. A shared settlement density scale was developed by applying figures compiled by Rice and Culbert (*35*) (Table 8). Their data, based on ground survey of sites with variably defined limits, provided the justification for four classes; a fifth—"vacant"—was added for a total of five classes. In summary, five structure

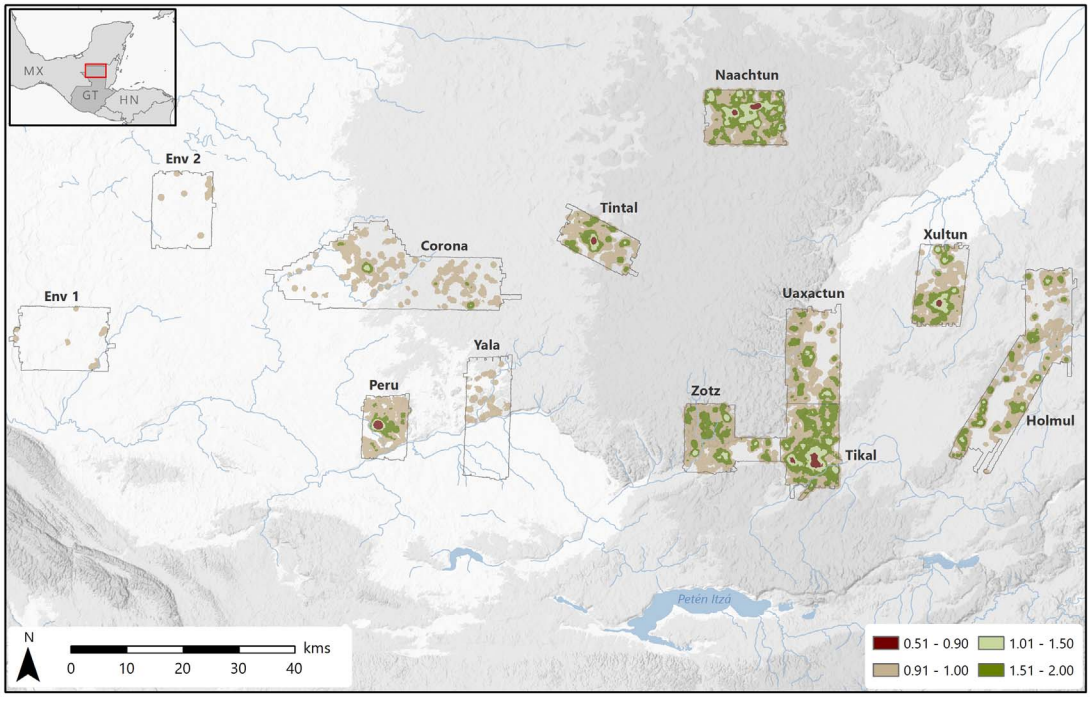

Fig. 6. Agricultural features relative to population densities. Map of survey blocks showing deviations from expected density of upland field areas relative to settlement density class area. Expected (i.e., "no difference") value is 1.0.

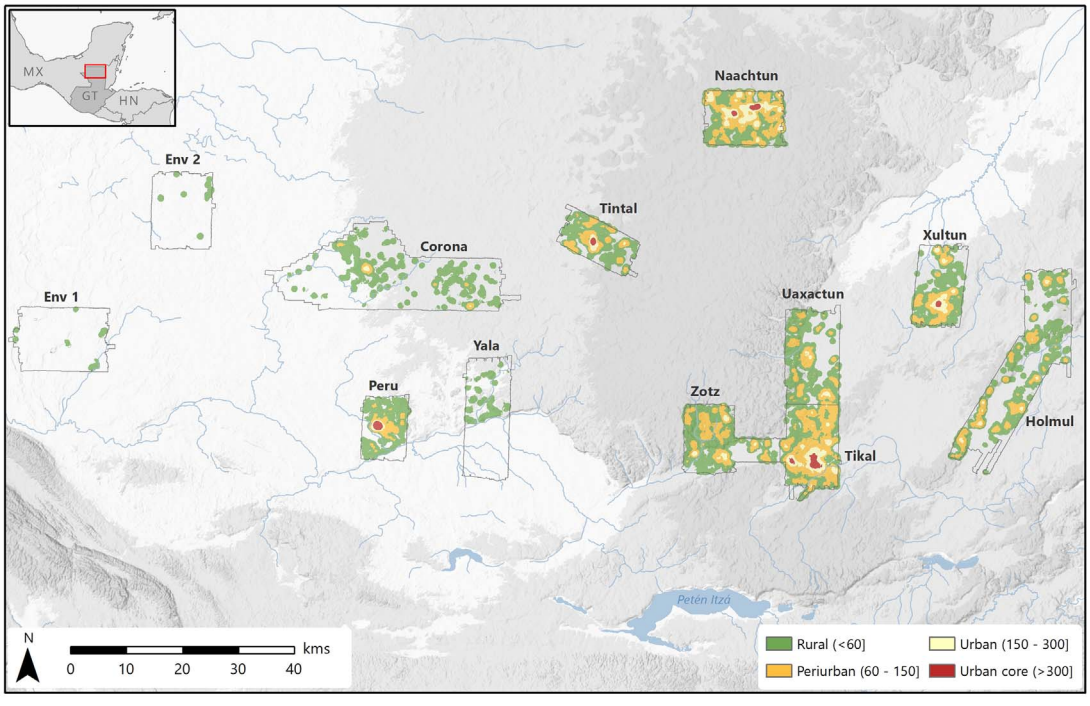

Fig. 7. Settlement density patterns. Density values are expressed as structures/km^2.

density categories—vacant, rural, periurban, urban, and urban core—were defined for the entire dataset (*29*) to discern differences not only in the size and density of cities but also in the relationship between cities and hinterlands (*86*–*89*).

The "urban core" class was defined on the basis of structure densities at the heart of the largest Maya centers, such as Tikal (~700 structures/km^2). "Urban" describes the structure density at the heart of many smaller cities within the PLI study area (e.g., Uaxactun, Zotz) as well as the densely settled surroundings of major cities' urban cores (e.g., Xultun, Naachtun, and Tikal). "Periurban" zones (also known in the literature as "urban fringes") combine characteristics of both urban and rural areas (*90*). The parameters of this category encompass those areas designated by prior surveys as "peripheral" to the largest Maya sites as well as sites often characterized as "minor centers" whose economic and political fortunes were closely articulated with larger cities nearby (*91*–*93*). Our "rural" class follows existing descriptions of settlement density in the hinterlands of smaller cities and minor centers. Finally, we classified as "vacant" all zones with fewer than 10 structures/km^2.

At the regional level, sprawling urban and periurban settlement zones covered large areas in the east, whereas the west remained mostly rural (Fig. 7). Urban core densities ran as high

Table 6. Maximum sustainable population of each survey block. Calculations designed to determine the maximum sustainable population within each survey block based on (i) its total measured agricultural area (values adjusted for Late Classic contemporaneity using AgroIndex) and (ii) a minimum swidden area of 0.48 ha/person (mean value of range reported in table S3).

Survey block	Uplands (ha)	Wetlands (adj. ha)	Modified uplands (adj. ha)	Pop. capacity (0.48 ha/person)	Population (*PopIndex* 3.16)	Under/over capacity	% capacity
Naachtun	3,387	2,288	2,574	17,062	37,889	20,827	222%
Tikal	6,069	407	4,305	22,298	38,892	16,594	174%
Xultun	1,992	0	2,847	10,008	17,438	7,430	174%
Perú	3,892	0	351	8,777	12,956	4,179	148%
Tintal	5,409	380	746	13,516	13,063	−453	97%
Uaxactun	4,238	281	3,958	17,532	16,052	−1,480	92%
Zotz	11,485	79	94	24,112	19,781	−4,331	82%
Holmul	12,866	1,350	2,322	34,206	22,796	−11,410	67%
Corona	19,399	0	14	40,150	11,478	−28,671	29%
Yala	7,738	0	82	16,172	2,341	−13,831	14%
Env 1	8,243	0	130	17,319	971	−16,347	6%
Env 2	10,487	52	44	21,887	803	−21,084	4%
PLI survey area	95,205	4,836	17,468	243,039	194,460	−48,579	0%

Table 7. Correlation of upland agricultural features with settlement density. Correlation matrix of intensive agriculture upland field zones and settlement density zones in m^2 (upland zones strongly correlate with periurban and urban zones; $N = 12$).

		Vacant	Rural	Periurban	Urban	Urban core	Intensive agr. fields
Vacant	Pearson correlation	1	0.612*	−0.368	−0.381	−0.460	−0.289
	Significance (two-tailed)		0.034	0.239	0.221	0.133	0.361
Rural	Pearson correlation	0.612*	1	0.278	−0.021	−0.152	0.248
	Significance (two-tailed)	0.034		0.382	0.949	0.637	0.438
Periurban	Pearson correlation	−0.368	0.278	1	0.835**	0.694*	0.749**
	Significance (two-tailed)	0.239	0.382		0.001	0.012	0.005
Urban	Pearson correlation	−0.381	−0.021	0.835**	1	0.775**	0.645*
	Significance (two-tailed)	0.221	0.949	0.001		0.003	0.023
Urban core	Pearson correlation	−0.460	−0.152	0.694*	0.775**	1	0.505
	Significance (two-tailed)	0.133	0.637	0.012	0.003		0.094
Upland area	Pearson correlation	−0.289	0.248	0.749**	0.645*	0.505	1
	Significance (two-tailed)	0.361	0.438	0.005	0.023	0.094	

*Correlation is significant at the 0.05 level (two-tailed). **Correlation is significant at the 0.01 level (two-tailed).

as 1000 to 2000 persons/km^2, whereas rural areas were as low as 50 persons/km^2 over continuous areas. However, the PLI sample also revealed striking regional differences in urbanization patterns (Table 9).

Cluster analysis of the settlement patterns within the PLI sample revealed several intraregional patterns. Because the PLI survey blocks varied in shape and in total area, standardized 80-km^2 sample areas were designed for cluster analysis. These areas were delineated to maintain the primary urban center in as central a location as possible within the sample area. Because of the variable shape and dimensions of each PLI survey block, sample areas could not be drawn with identical proportions; nonetheless, areas were 80 km^2 in all cases, with proportions as standardized as possible. The Corona and Holmul survey blocks were large enough to delineate two distinct sample areas for each survey block. These two additional sample areas were named Achiotal and Xmakabatun (for the Corona and Holmul survey blocks, respectively) after the name of the primary center within each area.

Cluster analysis of these 14 areas (Fig. 8) (*29*) indicates that settlement patterns at the regional level fall into three classes: (i) rural areas with low overall density and limited political integration (Env 1, Env 2, Yala, Corona, Achiotal); (ii) periurban areas containing small urban centers with large periurban and rural populations (Uaxactun, Holmul, Xmakabatun, and Zotz); and (iii) urban areas with periurban and rural populations surrounding and likely integrated with a single large urban center. Within this third class are two subclasses: moderately urbanized areas with more substantial periurban and rural populations (Tintal and Xultun), and highly urbanized areas in which most of the population lived in urban core, urban, and periurban zones (Naachtun and Tikal).

Such variety cannot be explained by sole reference to topographic, pedological, or ecological conditions; political and economic forces, including conflict, likely exerted commensurate or stronger influence. Furthermore, nearly all the areas identified as urban were also those incapable of sustaining themselves agriculturally, whereas all the rural and periurban areas were capable of producing food surpluses to feed the rest of the sample's population. These data suggest that lowland Maya settlement was characterized by both high variability and high interdependence along a rural-urban continuum rather than by a dispersed, homogeneous, low-density settlement (*94*).

Table 8. Late Classic structure density classes, modified from Rice and Culbert (*35*).

PLI density class		Site centers			Site peripheries			Rural	
Class	Density	Site	Area (km^2)	Density	Site	Area (km^2)	Density	Region	Density
Urban core	300+	Caracol	2.2	300					
		Tikal	9	235					
Urban	150–300	Ceibal	1.6	222					
		Becan	3	171	Tikal (16 km)	7	181		
		Tayasal	2.5	128	Ceibal	13.6	116	Belize Valley	116
Periurban	60–150	Cenote	0.5	128					
		Uaxactun	16	106					
								Tikal/Yaxha	60
		Nohmul	4	58				Lakes Macanche-Salpeten	57
								Lakes Yaxha-Sacnab	47
Rural	<60							Lakes Quexil-Petenxil	36
								Tikal (survey strips)	39
								Uaxactun	30
								Nohmul	12
Vacant	≤10								

Table 9. Relative frequency of structures in each density class by PLI survey block.

Name	Rural	Periurban	Urban	Urban core
Corona	81%	14%	5%	0%
Env 1	100%	0%	0%	0%
Env 2	100%	0%	0%	0%
Holmul	43%	48%	8%	0%
Naachtun	13%	41%	36%	10%
Perú	35%	24%	6%	34%
Tikal	12%	49%	25%	14%
Tintal	28%	48%	11%	12%
Uaxactun	46%	47%	7%	0%
Xultun	25%	42%	25%	7%
Yala	100%	0%	0%	0%
Zotz	36%	54%	11%	0%
All	30%	43%	18%	9%

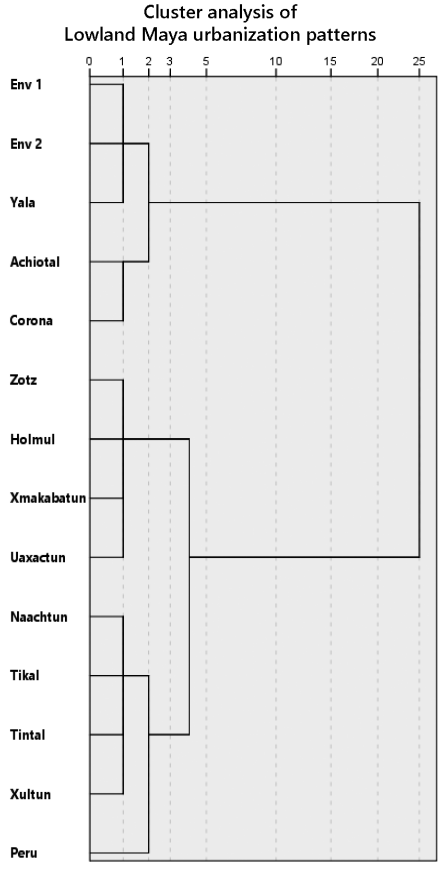

Fig. 8. Cluster analysis of density patterns. Ward linkage method, squared Euclidean distance.

A word of caution is warranted about assuming contemporaneity of all structures in this classification. For instance, three survey blocks—Zotz, Uaxactun, and Holmul—hold substantial centers that were abandoned in the Late Preclassic period and only partly resettled in the Classic period. However, because these blocks already form a statistically distinct group, we are confident that they would remain clustered even after factoring out all earlier settlement in those three areas.

A few other patterns bear mentioning. First, the city of El Perú-Waka' with a sustained density of 1100 structures/km^2 (*95*)—nearly double that of Tikal—exhibits a uniquely nucleated urban core that transitions rapidly to a rural hinterland. The singular urban morphology of El Perú-Waka', although it generally fits the urban area pattern, might reflect distinct economic or political influences on its development and organization. Second, although the Corona block was essentially rural, it did include several small pockets of urban density. This region had a strategic role in the expansion of the hegemonic Kaanul polity during the sixth through eighth centuries CE (*96*–*102*), so settlement nucleation here was probably conditioned by regional geopolitics in addition to local demographic processes. Finally, the urban and periurban settlement zones of Tikal extend over at least 76 km^2, representing one of the largest continuous settlement zones in the Maya Lowlands (*26*).

Engineering and infrastructure

Lidar data also elucidate the extent of lowland Maya investment in water management, regional communication, and defense. The Maya constructed reservoirs that required considerable labor (*103*). At the household level, reservoirs, quarries, wells, and underground cisterns were commonly cut into bedrock to collect rainwater (*104*–*110*). Within urban centers, the ancient Maya deepened, dammed, or bermed natural depressions to capture rainwater running off stucco-paved surfaces (*111*). Lidar data now show a greater extent of such large features. Large, round, and bermed reservoirs were built within

Table 10. Defensive data for individual defended areas. Summary of defensive data for individual defended areas and perimeter statistics. Bold lines separate different lidar survey blocks (in order as Yala, Tikal, Uaxactun, Holmul, Zotz, Xultun, Perú, Corona, and Tintal).

Site/region	Defended area	Number of defensive features	Number of defensive systems	Area (ha)	Length of all built defenses (m)	Total perimeter length (m)	Length of built perimeter defenses (m)	Length of natural perimeter defenses (m)	Total length of perimeter defenses (m)	% of perimeter with built defenses	% of perimeter with natural defenses	% of total perimeter defended
E4 River Site	Site core	4	4	7.5	727	1,170	727	443	1,170	62%	38%	100%
Tikal*	City extent	139	10	10,677.4	18,603	15,675	12,072	3,418	15,490	77%	22%	99%
Tikal Polity	Group NW of Tikal Wall	6	2	70.4	1,027	3,670	900	2,763	3,663	25%	75%	100%
Atalaya	Atalaya core	2	1	13.6	198	1,996	198	1,787	1,985	10%	90%	99%
RS028	Refuge	2	1	3.2	132	764	132	631	764	17%	83%	100%
RS07	Eastern hilltop	2	2	1.7	452	539	452	87	539	84%	16%	100%
Cival	Cival core	5	3	28.2	1,080	1,974	1,080	361	1,441	55%	18%	73%
Dos Aguadas	Dos Aguadas North E plateau	2	2	11.4	1,825	1,637	1,625	13	1,637	99%	1%	100%
Dos Aguadas	Dos Aguadas North N plateau	3	1	23.2	1,341	2,160	528	1,585	2,113	24%	73%	98%
Dos Aguadas	Dos Aguadas North W plateau	1	1	7.8	654	1,363	654	708	1,363	48%	52%	100%
Dos Aguadas	Dos Aguadas South core	14	7	52.1	3,391	3,660	1,650	1,861	3,511	45%	51%	96%
Dos Aguadas*	Dos Aguadas South macro	7	4	162.0	2,243	4,349	2,243	804	3,047	52%	18%	70%
Kanalna	Kanalna N refuge	2	1	7.1	287	1,280	116	1,164	1,280	9%	91%	100%
Kanalna	Kanalna S refuge	1	1	16.7	218	2,584	218	2,344	2,563	8%	91%	99%
La Sufricaya	La Sufricaya core	4	3	9.6	556	1,204	556	96	652	46%	8%	54%
Turca†	Turca core	1	1	—	99	—	—	—	—	—	—	—
Turca	Turca E refuge	2	1	2.8	271	695	148	547	695	21%	79%	100%
Witzna	Witzna core	3	1	44.0	547	4,254	200	3,011	3,211	5%	71%	75%
Witzna East	Witzna East	10	4	14.1	942	2,066	630	1,390	2,020	31%	67%	98%
Xmakabatun Polity	Summit E of drainage	6	4	2.9	881	746	412	181	594	55%	24%	80%
Xmakabatun Polity	Summit W of drainage	1	1	5.4	525	924	525	213	738	57%	23%	80%
El Zotz	El Diablo	15	4	21.6	3,347	2,403	1,829	471	2,300	76%	20%	96%
El Zotz	El Tejon	11	3	9.3	1,717	1,399	542	805	1,346	39%	58%	96%
El Zotz	Hill NW of El Diablo Group	5	1	0.9	332	480	148	332	480	31%	69%	100%
El Zotz Polity‡	Drainage N of La Cuernavilla	6	1	10.4	437	1,106	—	—	—	—	—	—
El Zotz Polity	Hills at N drainage intersection	3	2	15.3	771	1,966	771	1,191	1,962	39%	61%	100%
El Zotz Polity	Hills W of La Cuernavilla	7	3	11.5	1,035	2,904	602	2,293	2,895	21%	79%	100%
La Cuernavilla	La Cuernavilla East	27	6	55.0	5,014	4,222	1,278	1,777	3,055	30%	42%	72%
La Cuernavilla	La Cuernavilla West	24	3	21.7	4,262	2,697	1,777	722	2,499	66%	27%	93%
Xultun Polity‡	City extent	21	1	—	298	—	—	—	—	—	—	—
Xultun Polity‡	Unknown	2	1	—	332	—	—	—	—	—	—	—
El Perú-Waka'	El Perú-Waka' core	3	2	164.1	1,100	5,193	1,100	2,151	3,251	21%	41%	63%
El Perú-Waka' Polity‡	Territorial extent	1	1	—	1,240	—	—	—	—	—	—	—
El Achiotal Polity	Defensive enclosure	10	1	1.8	827	522	505	0	505	97%	0%	97%
El Achiotal Polity	Peninsula refuge	3	1	16.7	554	2,193	354	1,792	2,145	16%	82%	98%
Tintal	Tintal core	15	3	37.3	2,703	2,481	1,811	452	2,263	73%	18%	91%

*The defended area extends beyond the limits of the lidar data, but a substantial portion is visible. All statistics are based on the visible perimeter and area, but may not be reliable metrics of the actual defended area. †There is no clearly discernible defended area for the defensive systems present. Area not included in comparative analyses. ‡The defended area extends beyond the limits of the lidar data and is too incomplete to include in comparative analyses.

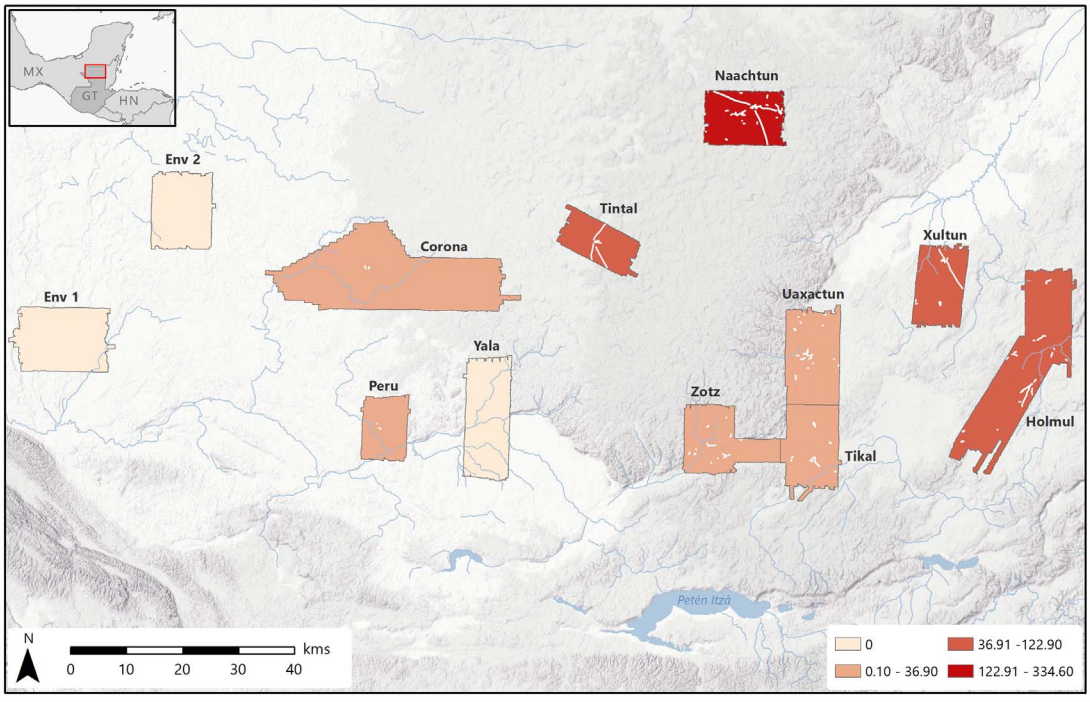

Fig. 9. Map of survey blocks showing causeway density patterns. Causeways are shown in white; values represent cumulative causeway length (in meters) normalized by survey block area (km^2).

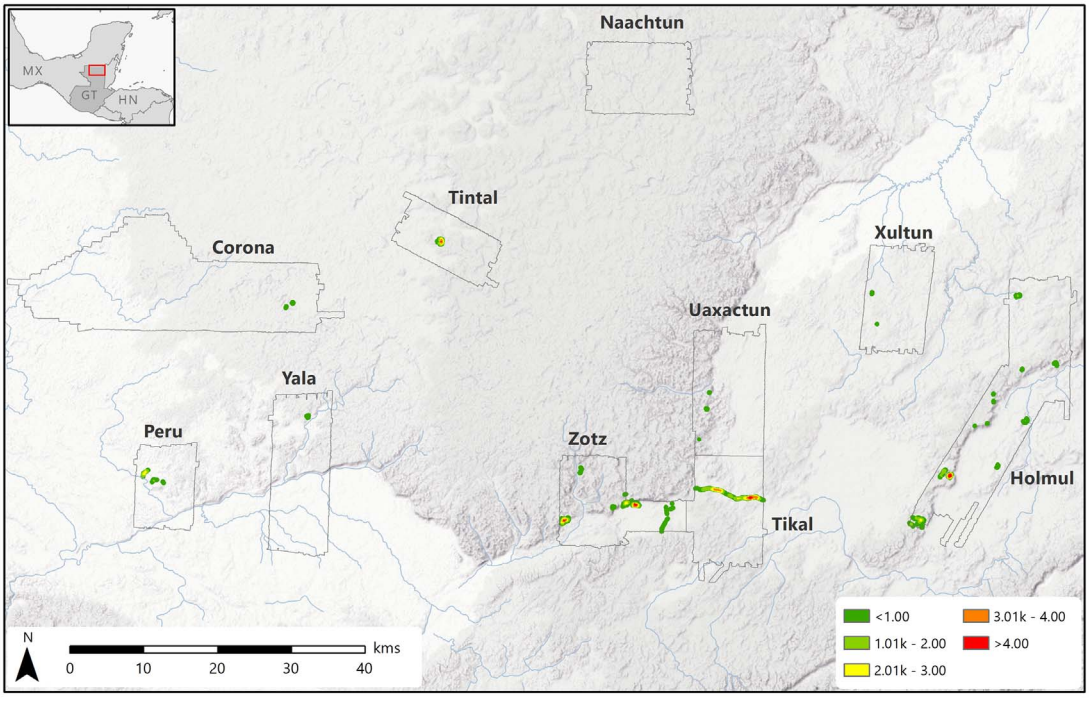

Fig. 10. Density of defensive features. Density is expressed as linear meters of defensive features per square kilometer normalized by survey block area.

wetlands to serve the needs of the rural population, and drainage ditches were cut into the edges of reservoirs to control flow during the wettest periods.

Lidar-derived terrain models allow for a volumetric assessment of reservoirs, in measures likely to be conservative because of later infilling. Here, we present data only on the built reservoirs of large scale (i.e., those serving more than a single household) (*29*). In our sample, Tikal's urban core had the largest amount of water storage capacity in human-made reservoirs. The Tikal Palace Reservoir alone could store 31,000 m^3 of water, which would be sufficient to supply the inhabitants of the urban core for an entire year. Earlier cities such as Cival and Tintal were near natural depressions that provided generous amounts of water with little labor investment. For example, Tintal ringed a 2-km-wide sinkhole that could have contained more than 3 million m^3 of water in wet years. A 2.5-km canal carried overflow into a natural drainage, preventing rising waters from flooding the city.

In all cases, such features are monumental in scale and imply some form of centralized involvement in planning and execution. Notably, large-scale water infrastructure is not limited to city centers but occurs in the periurban and even rural zones surrounding major cities, and

in some cases integrates cities and their peripheries. These findings indicate that the construction of monumental reservoirs and, less commonly, canals in both city centers and rural areas involved some form of centralized, institutional coordination. Yet this observation does not negate the possibility that smaller-scale infrastructure was independently built by households and corporate groups (*104*). Rather, the PLI data suggest that water management was neither fully centralized (*112*) nor left completely to individual households.

Lidar data also reveal investment in regional and local interconnectivity. "Causeways," elevated and paved roads of varied size, demonstrate economic and political integration by revealing formal connections between cities, smaller communities, and dispersed populations (*113*). Until recently, knowledge of formal political connections was restricted to epigraphic records of dynastic interaction and a small number of causeways (*25*, *26*, *114*–*117*). The lidar sample identified ~106 linear kilometers of causeway construction dating to the Late Preclassic and Classic periods. Intersite causeways are primarily associated with cities that rose to prominence during the Preclassic period (Tintal, Cival, San Bartolo) or Early Classic (Naachtun) and are surprisingly absent from the Late Classic period. They can reach up to 22 km in length (Tintal-Mirador) and 10 to 20 m in width, linking cities to smaller centers nearby. Examples of these occur at Tintal, where multiple monumental causeways radiate toward other centers. Intra-site causeways are associated with Late Classic period centers of all sizes. These roads are typically only a few hundred meters long, providing grand entryways to public spaces within a community. Tikal has the widest causeways (80 m) and the largest amount of internal paved causeway area (0.19 km^2). Overall, causeways are more widely distributed than had been previously appreciated, especially in the Late Classic period. Across the sample, there is a general trend of increased causeway density from west to east and from south to north (Fig. 9), coinciding with regional gradients in settlement density, agricultural intensification, and water management infrastructure.

Perhaps the most obvious example of infrastructural investment comes in the form of defensive or military features pointing to a high incidence of conflict in the Maya Lowlands. Such fortifications are found at a scale and quantity (Fig. 10) matched only by the Tikal earthworks and the monumental fortifications at Becan, both known since the 1960s (*118*–*120*). To a notable extent, settlement density does not correlate with regional defense, in that some of the most densely settled blocks, such as Naachtun, have no defensive features. Individual defensive features—bridges, ditches, ramparts, stone walls, and terraces—were constructed as components of "built defensive systems." These combined with natural defenses to protect "defended areas." There were five types of built defensive systems: landscape ditch-and-rampart (type 1), hilltop ditch-and-rampart (type 2),

Table 11. Statistics for reinforcing defenses. Bold lines define natural breaks (Jenks) in the percentages of additional defenses in relation to an area's perimeter.

Site/region	Defended area	Length of additional defenses (m)	% of additional defenses from total built	% of additional defenses from total perimeter
La Cuernavilla	La Cuernavilla East	3736	75%	122%
La Cuernavilla	La Cuernavilla West	2485	58%	99%
El Zotz	El Tejon	1176	68%	87%
Tintal	Tintal core	1811	67%	80%
Xmakabatun Polity	Summit E of drainage	469	53%	79%
El Zotz	El Diablo	1519	45%	66%
El Achiotal Polity	Defensive enclosure	321	39%	64%
Dos Aguadas	Dos Aguadas South core	1742	51%	50%
Tikal*	City extent	6531	35%	42%
Dos Aguadas	Dos Aguadas North N plateau	813	61%	38%
El Zotz	Hill NW of El Diablo Group	184	55%	38%
Turca	Turca E refuge	123	45%	18%
Witzna East	Witzna East	312	33%	15%
El Zotz Polity	Hills W of La Cuernavilla	433	42%	15%
Kanalna	Kanalna N refuge	171	60%	13%
Dos Aguadas	Dos Aguadas North E plateau	200	11%	12%
Witzna	Witzna core	347	63%	11%
El Achiotal Polity	Peninsula refuge	200	36%	9%
Tikal Polity	Group NW of Tikal Wall	127	12%	3%
RS028	Refuge	0	0%	0%
Dos Aguadas	Dos Aguadas North W plateau	0	0%	0%
RS07	Eastern hilltop	0	0%	0%
E4 River Site	Site core	0	0%	0%
El Zotz Polity	Hills at N drainage intersection	0	0%	0%
Atalaya	Atalaya core	0	0%	0%
Kanalna	Kanalna S refuge	0	0%	0%
Xmakabatun Polity	Summit W of drainage	0	0%	0%
Cival	Cival core	0	0%	0%
Dos Aguadas*	Dos Aguadas South macro	0	0%	0%
El Perú-Waka'	El Perú-Waka' core	0	0%	0%
La Sufricaya	La Sufricaya core	0	0%	0%

*The defended area extends beyond the limits of the lidar data, but a substantial portion is visible.

contoured terrace (type 3), stand-alone rampart (type 4), and stone wall (type 5). These were unevenly distributed across the sample, reflecting variation in local geography, resources, and history.

Built defensive systems are found in 36 discrete locations across the sample, with 31 meeting the criteria for defended areas (Table 10). In most cases (61.3%), defenses consisted of more than the establishment of perimeter walls. One-third (n = 10) of all defended areas displayed more defensive features within the perimeter than on the perimeter itself (Table 11). The Holmul and Zotz survey blocks exhibited the greatest effort in reinforcing defenses, suggesting a heavy investment in the protection of particular sites in those areas. We also identified "refuges," highly defensible areas lacking any other perceptible architecture. Presumably, these were only used as a last resort and for brief stays. Clear examples appear at Kanalna and the El Achiotal promontory.

Several metrics were calculated to interpret the defensive data (*29*). We assessed the "perceived need" for defense of an area according to the percentage of the perimeter defended by built or natural defenses (Table 10), as well as how much defensibility factored into the siting of a settlement. The latter statistic is a preparedness index that factors out the natural defensibility of a location (Table 12). At some larger sites, such as Tikal and Tintal, substantial investment in building perimeter defenses around the urban core suggests that the need for such constructions emerged well after the initial establishment of the settlement. Finally, we assessed the cost of building defensive systems in relation to the total protected area (Table 13). The defensive features of greatest cost are located in the southern part of the sample, particularly the Early Classic Buenavista Valley linking El Zotz and Tikal.

At the regional level, the Zotz, Tikal, Holmul, and Perú blocks show the greatest concentration of defensive features (Table 14). However, both the Zotz and Tikal regions demonstrate the largest investment of built and combined defenses in the sample. By controlling for survey block size, a line density analysis (Fig. 10) highlights the higher investment in defense along a west-to-east route. The trend continues to the east with several fortified hilltops in the Holmul region. The greatest density of high-cost features extends along a corridor associated with a Central Mexican (Teotihuacan) military intrusion into the Maya Lowlands in the late fourth century CE (*121*).

Concluding remarks

Since its first application in Maya archaeology (*122*), lidar technology has enabled the evaluation of lowland Maya society on a large scale. The PLI results confirm that lidar technology represents a watershed event in archaeological survey of forested environments. In the central Maya Lowlands, lidar survey will become indispensable for settlement research because of (i) the speed of the data-gathering process, (ii) the degree of detail attainable over large areas, and (iii) the ability to discern large and small features routinely undetected by traditional methods.

The PLI lidar survey provides a uniquely large and continuous dataset for the central Maya Lowlands that is replete with evidence for ancient structures, canals, terraces, causeways, and defensive features. These data also show great variability in the intensity and distribution of these features over space. In sum, the PLI data unambiguously support the notion that the lowland Maya constructed a variable and contentious landscape in which a regionally interconnected network of densely populated and defended cities was sustained by an array of agricultural practices that optimized land productivity, resource diversity, and sustainability on a much grander scale than previously thought.

These preliminary conclusions should encourage research that, among many possibilities, (i) quantifies labor investments and land productivity at every scale; (ii) addresses how projects of agricultural intensification were organized and managed, with implications for long-term sustainability; (iii) assesses the extent of economic interdependence within large regions by studying differences between urban and rural populations; (iv) determines the relationship among settlement densities, land use, and monumental infrastructure; and (v) develops models for the types of warfare implied by defensive features.

Finally, by detecting most looters' pits and assembling full inventories of ruins, lidar data offer a profound tool for cultural heritage management. Quantification of biomass and monitoring of biodiversity—an underexplored product of these lidar data—will also facilitate planning and management of regional conservation efforts and deepen our understanding of the relationship between ancient and modern environments.

Methods

The Pacunam Lidar Initiative collected lidar data over an area of 2144 km^2 of the Maya Biosphere

Table 12. Degree of preparedness for each defended area. The degree to which the need for defense was anticipated at the time of initial settlement. Scores closer to 0 indicate minimal preparedness.

Site/region	Defended area	Preparedness index
El Zotz	Hill NW of El Diablo Group	369
RS028	Refuge	199
El Zotz Polity	Hills W of La Cuernavilla	199
Turca	Turca E refuge	194
Kanalna	Kanalna N refuge	164
Kanalna	Kanalna S refuge	140
Atalaya	Atalaya core	132
El Achiotal Polity	Peninsula refuge	107
Witzna East	Witzna East	99
Dos Aguadas	Dos Aguadas North W plateau	91
El Zotz	El Tejon	87
El Zotz Polity	Hills at N drainage intersection	78
Witzna	Witzna core	68
Dos Aguadas	Dos Aguadas North N plateau	68
Xmakabatun Polity	Summit E of drainage	62
E4 River Site	Site core	59
RS07	Eastern hilltop	50
Xmakabatun Polity	Summit W of drainage	39
Tikal Polity	Group NW of Tikal Wall	39
Dos Aguadas	Dos Aguadas South core	36
La Cuernavilla	La Cuernavilla West	33
La Cuernavilla	La Cuernavilla East	32
El Zotz	El Diablo	22
El Perú-Waka'	El Perú-Waka' core	13
Cival	Cival core	13
Tintal	Tintal core	12
La Sufricaya	La Sufricaya core	10
Dos Aguadas*	Dos Aguadas South macro	5
Dos Aguadas	Dos Aguadas North E plateau	1
Tikal*	City extent	0
El Achiotal Polity	Defensive enclosure	0

*The defended area extends beyond the limits of the lidar data, but a substantial portion is visible.

Table 13. Cost index for each defended area. Cost statistics for defending areas in relation to idealized forms.

Site/region	Defended area	Total built defenses (m)	z-score of TBD	Overbuild score	Efficiency score	Cost index
La Cuernavilla	La Cuernavilla West	4,262	0.73	2.58	0.61	3.08
La Cuernavilla	La Cuernavilla East	5,014	0.96	1.91	0.62	2.94
El Zotz	El Diablo	3,348	0.45	2.03	0.69	1.34
Tikal*	City extent	18,603	5.09	0.51	2.34	1.11
Dos Aguadas	Dos Aguadas South core	3,391	0.47	1.33	0.70	0.88
Tintal	Tintal core	2,703	0.26	1.25	0.87	0.37
Dos Aguadas*	Dos Aguadas South macro	2,243	0.12	0.50	1.04	0.06
Dos Aguadas	Dos Aguadas North E plateau	1,825	−0.01	1.52	0.73	−0.02
El Perú-Waka'	El Perú-Waka' core	1,100	−0.23	0.24	0.87	−0.06
El Zotz	El Tejon	1,717	−0.04	1.59	0.77	−0.09
Tikal Polity	Group NW of Tikal Wall	1,027	−0.25	0.35	0.81	−0.11
Atalaya	Atalaya core	198	−0.50	0.15	0.65	−0.12
RS028	Refuge	132	−0.52	0.21	0.83	−0.13
Kanalna	Kanalna S refuge	218	−0.50	0.15	0.56	−0.13
Cival	Cival Core	1,080	−0.24	0.57	0.95	−0.14
Dos Aguadas	Dos Aguadas North N plateau	1,341	−0.16	0.78	0.79	−0.16
Witzna	Witzna core	547	−0.40	0.23	0.55	−0.17
Kanalna	Kanalna N refuge	287	−0.48	0.30	0.74	−0.20
La Sufricaya	La Sufricaya core	556	−0.40	0.51	0.91	−0.22
El Achiotal Polity	Peninsula refuge	554	−0.40	0.38	0.66	−0.23
Turca	Turca E refuge	271	−0.48	0.45	0.86	−0.26
El Zotz Polity	Hills at N drainage intersection	771	−0.33	0.56	0.71	−0.26
Xmakabatun Polity	Summit W of drainage	525	−0.40	0.64	0.89	−0.29
Witzna East	Witzna East	942	−0.28	0.71	0.64	−0.31
E4 River Site	Site core	727	−0.34	0.75	0.83	−0.31
Dos Aguadas	Dos Aguadas North W plateau	654	−0.37	0.66	0.73	−0.33
RS07	Eastern hilltop	452	−0.43	0.97	0.86	−0.48
El Zotz Polity	Hills W of La Cuernavilla	1,035	−0.25	0.86	0.41	−0.52
Xmakabatun Polity	Summit E of drainage	881	−0.30	1.46	0.81	−0.53
El Achiotal Polity	Defensive enclosure	827	−0.31	1.73	0.91	−0.59
El Zotz	Hill NW of El Diablo Group	332	−0.46	0.99	0.70	−0.65

*The defended area extends beyond limits of lidar data, but a substantial portion is visible.

Table 14. Regional defensive statistics by lidar survey block. TLD, total length defended; TBD, total built defenses.

Polygon	Major site	Lidar area (km^2)	Number of defensive systems	km^2 of lidar per defensive system	Number of defensive features	km^2 of lidar per defensive feature	Total length of defended perimeters (m)	Length of defended perimeter per km^2 of lidar	Defended area (km^2)	% lidar area defended	TLD (m)	TLD per km^2 of lidar	TBD length (m)	TBD per km^2 of lidar
E1		184.14	0	0.0	0	0.0	0	0	0.0	0.0%	0	0.0	0	0.0
E2		145.59	0	0.0	0	0.0	0	0	0.0	0.0%	0	0.0	0	0.0
E4		172.02	4	43.0	4	43.0	1,170	7	0.1	0.0%	1,170	6.8	727	4.2
1	Tikal	161.33	12	13.4	145	1.1	19,345	120	107.5	66.6%	25,811	160.0	19,630	121.7
2	Uaxactun	164.94	4	41.2	6	27.5	3,298	20	0.2	0.1%	3,287	19.9	782	4.7
8	Naachtun	135.26	0	0.0	0	0.0	0	0	0.0	0.0%	0	0.0	0	0.0
9	Holmul	308.66	35	8.8	62	5.0	28,895	94	3.9	1.3%	29,139	94.4	14,862	48.1
10	El Zotz	127.20	23	5.5	98	1.3	17,922	141	1.5	1.1%	24,507	192.7	16,915	133.0
11	Xultun	124.02	2	62.0	23	5.4	0	0	0.0	0.0%	630	5.1	630	5.1
12	El Perú	90.96	3	30.3	4	22.7	5,193	57	1.6	1.8%	4,491	49.4	2,340	25.7
13	La Corona	424.69	2	212.3	13	32.7	2,715	6	0.2	0.0%	3,173	7.5	1,381	3.3
15	Tintal	97.03	3	32.3	15	6.5	2,481	26	0.4	0.4%	3,155	32.5	2,703	27.9
Total		2,135.84	88	24.3	370	5.8	81,019	38	115.3	5.4%	95,363	44.6	59,971	28.1
Average		177.99	7.33	37.4	30.83	12.1	6,752	39	9.6	6.0%	7,947	47.4	4,998	31.1

Reserve (MBR) in northern Guatemala. These data were provided to the research consortium as bare-earth terrain models with grid resolution of 1 m. Given the coverage scale and resolution, these raster models make it possible to interpret aspects of ancient Maya society as warranted by visible remains of archaeological settlement. These data were analyzed to (i) estimate regional population levels, (ii) calculate agricultural capacity, (iii) determine settlement density patterns, and (iv) evaluate the extent of infrastructural investment in water storage, regional communication, and defense.

Terrain data and its derivatives were mostly manipulated and analyzed through GIS applications (ArcMap 10.4 and 10.6, QGIS 2.18, and GRASS 7.2, and the Relief Visualization Toolkit 1.3), enhanced by supplemental calculations and statistical analyses performed in Microsoft Excel and SPSS. Terrain models were visualized using multiple methods. Archaeological features were digitized manually, using existing site maps as training samples, augmented by targeted ground-truthing during the 2017 field season. All PLI member projects uploaded their manually derived feature datasets to a shared cloud server, where they were collated to create a single regional dataset for each feature class (e.g., buildings, causeways, terraces, etc.).

Population estimates are based on the total number of structures in the sample and include adjustments for Late Classic occupation, nonresidential structures, structures not visible on the surface, contemporaneity of occupation within the Late Classic period, and number of persons per structure. Settlement density classes were calculated using the Heatmap tool in QGIS 2.18 and classified according to published descriptions of settlement density in the cores and peripheries of numerous sites in the central Lowlands. Agricultural capacity was estimated by combining zones of intensive cultivation (defined on the basis of built agricultural features) with sparsely settled and unmodified uplands to define the total area available for agriculture; this area was then multiplied by a standardized estimate of traditional Maya swidden productivity. Water storage capacity was calculated using the r.lake function in GRASS 7.2. Causeways were classified using published typologies and statistics calculated by "calculate geometries" in ArcMap 10.4. Defensive features were classified by an original typology, their distribution was analyzed using the Line Density tool in ArcMap 10.6, and inferences regarding their cost effectiveness and other metrics were derived from statistical analyses performed in Microsoft Excel.

See (*29*) for detailed methodology and analytical procedures for each of these analyses.

REFERENCES AND NOTES

1. A. H. Siemens, in *Pre-Hispanic Maya Agriculture*, P. D. Harrison, B. L. Turner II, Eds. (Univ. of New Mexico Press, 1978), pp. 117–143.
2. T. Inomata *et al*., Archaeological application of airborne lidar with object-based vegetation classification and visualization techniques at the lowland Maya site of Ceibal, Guatemala. *Remote Sens.* **9**, 563 (2017). doi: 10.3390/rs9060563
3. A. F. Chase *et al*., Airborne lidar, archaeology, and the ancient Maya landscape at Caracol, Belize. *J. Archaeol. Sci.* **38**, 387–398 (2011). doi: 10.1016/j.jas.2010.09.018
4. K. Reese-Taylor *et al*., Boots on the ground at Yaxnohcah: Ground-truthing LiDAR in a complex tropical landscape. *Adv. Archaeol. Pract.* **4**, 314–338 (2016). doi: 10.7183/2326-3768.4.3.314
5. A. F. Chase *et al*., Ancient Maya regional settlement and inter-site analysis: The 2013 west-central Belize lidar survey. *Remote Sens.* **6**, 8671–8695 (2014). doi: 10.3390/rs6098671
6. A. F. Chase *et al*., The Use of LiDAR in Understanding the Ancient Maya Landscape: Caracol and Western Belize. *Adv. Archaeol. Pract.* **2**, 147–160 (2014). doi: 10.7183/2326-3768.4.3.314
7. J. Yaeger, M. K. Brown, B. Cap, Locating and dating sites using lidar survey in a mosaic landscape in western Belize. *Adv. Archaeol. Pract.* **4**, 339–356 (2016). doi: 10.7183/2326-3768.4.3.339
8. A. Ford, Using cutting-edge lidar technology at El Pilar Belize-Guatemala in discovering ancient Maya sites—there is still a need for archaeologists. *Res. Rep. Belizean Archaeol.* **12**, 271–280 (2014).
9. B. L. Turner 2nd, J. A. Sabloff, Classic Period collapse of the Central Maya Lowlands: Insights about human-environment relationships for sustainability. *Proc. Natl. Acad. Sci. U.S.A.* **109**, 13908–13914 (2012). doi: 10.1073/pnas.1210106109; pmid: 22912403
10. N. Grube, in *A Comparative Study of Thirty City-State Cultures*, H. M. Hansen, Ed. (Royal Danish Academy of Sciences and Letters, 2000), pp. 547–565.
11. D. L. Webster, in *The Archaeology of City-States: Cross-Cultural Approaches*, D. L. Nichols, T. H. Charlton, Eds. (Smithsonian Institution Press, 1997), pp. 135–154.
12. D. A. Freidel, in *Peer-Polity Interaction and Socio-political Change*, C. Renfrew, J. F. Cherry, Eds. (Cambridge Univ. Press, 1986), pp. 93–108.
13. T. P. Culbert, *Ancient Maya Wetland Agriculture* (Foundation for the Advancement of Mesoamerican Studies, 2005); www.famsi.org/reports/94033/index.html.
14. S. L. Fedick, in *The Managed Mosaic: Ancient Maya Agriculture and Resource Use*, S. L. Fedick, Ed. (Univ. of Utah Press, 1996), pp. 107–131.
15. N. P. Dunning *et al*., Arising from the *bajos*: The evolution of a neotropical landscape and the rise of Maya civilization. *Ann. Assoc. Am. Geogr.* **92**, 267–283 (2002). doi: 10.1111/1467-8306.00290
16. P. D. Harrison, in *Social Process in Maya Prehistory: Studies in Honour of Sir Eric Thompson*, N. Hammond, Ed. (Academic Press, 1977), pp. 469–508.
17. J. L. Kunen, P. T. Culbert, V. Fialko, B. M. McKee, L. Grazioso, Bajo communities: A case study from the central Peten. *Cult. Agric.* **22**, 15–31 (2000). doi: 10.1525/cag.2000.22.3.15
18. M. D. Pohl, Ed., *Ancient Maya Wetland Agriculture: Excavations on Albion Island, Northern Belize* (Westview, 1990).
19. N. P. Dunning, T. Beach, Soil erosion, slope management, and ancient terracing in the Maya Lowlands. *Lat. Am. Antiq.* **5**, 51–69 (1994). doi: 10.2307/971902
20. A. F. Chase, D. Z. Chase, Scale and intensity in Classic period Maya agriculture: Terracing and settlement at the 'garden city' of Caracol, Belize. *Cult. Agric.* **20**, 60–77 (1998). doi: 10.1525/cag.1998.20.2-3.60
21. N. P. Dunning, T. Beach, D. Rue, The paleoecology and ancient settlement of the Petexbatun region, Guatemala. *Anc. Mesoam.* **8**, 255–266 (1997). doi: 10.1017/S0956536100001711
22. D. Z. Chase, A. F. Chase, W. A. Haviland, The Classic Maya city: Reconsidering the "Mesoamerican urban tradition". *Am. Anthropol.* **92**, 499–506 (1990). doi: 10.1525/aa.1990.92.2.02a00210
23. A. F. Chase, D. Z. Chase, Ancient Maya causeways and site organization at Caracol, Belize. *Anc. Mesoam.* **12**, 273–281 (2001). doi: 10.1017/S0956536101121097
24. W. J. Folan, Calakmul, Campeche: A centralized urban administrative center in the northern Petén. *World Archaeol.* **24**, 158–168 (1992). doi: 10.1080/00438243.1992.9980199
25. S. Martin, N. Grube, *Chronicle of the Maya Kings and Queens* (Thames & Hudson, ed. 2, 2008).
26. D. Z. Chase, A. F. Chase, Caracol, Belize, and changing perceptions of ancient Maya society. *J. Archaeol. Res.* **25**, 185–249 (2017). doi: 10.1007/s10814-016-9101-z
27. B. L. Turner II, in *Culture, Form, and Place: Essays in Cultural and Historical Geography*, K. W. Mathewson, Ed. (Louisiana State University, 1993), pp. 57–88.
28. J. C. Fernandez-Diaz *et al*., Capability assessment and performance metrics for the Titan multispectral mapping lidar. *Remote Sens.* **8**, 936 (2016). doi: 10.3390/rs8110936
29. See supplementary materials.
30. K. Zakšek, K. Oštir, Ž. Kokalj, Sky-View Factor as a relief visualization technique. *Remote Sens.* **3**, 398–415 (2011). doi: 10.3390/rs3020398
31. T. Chiba, S.-i. Kaneta, Y. Suzuki, Red relief image map: New visualization method for three dimensional data. *Int. Arch. Photogramm. Remote Sens. Spat. Inf. Sci.* **37**, 1071–1076 (2008).
32. Ž. Kokalj, R. Hesse, *Airborne Laser Scanning Raster Data Visualization: A Guide to Good Practice* (Založba ZRC, Ljubljana, 2017).
33. M. Doneus, Openness as visualization technique for interpretative mapping of airborne lidar derived digital terrain models. *Remote Sens.* **5**, 6427–6442 (2013). doi: 10.3390/rs5126427
34. D. S. Rice, in *Urbanism in the Preindustrial World: Cross-Cultural Approaches*, G. R. Storey, Ed. (Univ. of Alabama Press, 2006), pp. 252–276.
35. D. S. Rice, T. P. Culbert, in *Precolumbian Population History in the Maya Lowlands*, T. P. Culbert, D. S. Rice, Eds. (Univ. of New Mexico Press, 1990), pp. 1–36.
36. B. L. Turner II, in *Precolumbian Population History in the Maya Lowlands*, T. P. Culbert, D. S. Rice, Eds. (Univ. of New Mexico Press, 1990), pp. 301–324.
37. A. Ford, R. Nigh, *The Maya Forest Garden: Eight Millennia of Sustainable Cultivation of the Tropical Woodlands* (Routledge, 2015).
38. T. Inomata *et al*., Archaeological application of airborne LiDAR to examine social changes in the Ceibal region of the Maya lowlands. *PLOS ONE* **13**, e0191619 (2018). doi: 10.1371/journal.pone.0191619; pmid: 29466384
39. R. E. W. Adams, in *Lowland Maya Settlement Patterns*, W. A. Ashmore, Ed. (Univ. of New Mexico Press, 1981), pp. 211–257.
40. T. P. Culbert, The new Maya. *Archaeology* **51**, 48–51 (1998).
41. R. J. Sharer, L. P. Traxler, *The Ancient Maya* (Stanford Univ. Press, 2006).
42. S. G. Ortman, A. H. F. Cabaniss, J. O. Sturm, L. M. A. Bettencourt, The pre-history of urban scaling. *PLOS ONE* **9**, e87902 (2014). doi: 10.1371/journal.pone.0087902; pmid: 24533062
43. P. D. Harrison, B. L. Turner II, Eds., *Pre-Hispanic Maya Agriculture* (Univ. of New Mexico Press, 1978).
44. J. L. Kunen, Ancient Maya agricultural installations and the development of intensive agriculture in N.W. Belize. *J. Field Archaeol.* **28**, 325–346 (2001). doi: 10.1179/jfa.2001.28.3-4.325
45. D. L. Lentz *et al*., Forests, fields, and the edge of sustainability at the ancient Maya city of Tikal. *Proc. Natl. Acad. Sci. U.S.A.* **111**, 18513–18518 (2014). doi: 10.1073/pnas.1408631111; pmid: 25512500
46. N. P. Dunning *et al*., in *Tikal: Paleoecology of an Ancient Maya City*, D. L. Lentz, V. L. Scarborough, N. P. Dunning, Eds. (Cambridge Univ. Press, 2015), pp. 95–123.
47. R. E. W. Adams, Swamps, canals, and the location of ancient Maya cities. *Antiquity* **54**, 206–214 (1980). doi: 10.1017/S0003598X00043386
48. R. E. W. Adams, W. E. Brown Jr., T. P. Culbert, Radar mapping, archeology, and ancient Maya land use. *Science* **213**, 1457–1468 (1981). doi: 10.1126/science.213.4515.1457; pmid: 17780866
49. R. E. W. Adams, T. P. Culbert, W. E. Brown Jr., P. D. Harrison, L. J. Levy, Rebuttal to Pope and Dahlin. *J. Field Archaeol.* **17**, 241–243 (1990).
50. K. O. Pope, B. H. Dahlin, Ancient Maya wetland agriculture: New insights from ecology and remote sensing research. *J. Field Archaeol.* **16**, 87–106 (1989).
51. N. P. Dunning, in *The Managed Mosaic: Ancient Maya Agriculture and Resource Use*, S. L. Fedick, Ed. (Univ. of Utah Press, 1996), pp. 53–68.
52. K. O. Pope, B. H. Dahlin, Radar detection and ecology of ancient Maya canal systems—Reply to Adams *et al*. *J. Field Archaeol.* **20**, 379–383 (1993). doi: 10.2307/530065
53. B. L. Turner II, in *Pre-Hispanic Maya Agriculture*, P. D. Harrison, B. L. Turner II, Eds. (Univ. of New Mexico Press, 1978), pp. 163–183.
54. P. D. Harrison, in *Vision and Revision in Maya Studies*, F. S. Clancy, P. D. Harrison, Eds. (Univ. of New Mexico Press, 1990), pp. 99–113.
55. T. P. Culbert, L. Levi, L. Cruz, in *Vision and Revision in Maya Studies*, F. S. Clancy, P. D. Harrison, Eds. (Univ. of New Mexico Press, 1990), pp. 115–124.

56. T. P. Culbert, L. J. Levi, B. M. McKee, J. L. Kunen, in *IX Simposio de Investigaciones Arqueológicas en Guatemala*, J. P. Laporte, H. L. Escobedo, Eds. (Instituto Nacional de Antropología e Historia, Guatemala, 1996), pp. 51–57.
57. B. H. Dahlin, A. Dahlin, Platforms in the *akalche* at El Mirador, Peten, Guatemala and their implications. *Geoarchaeology* **9**, 203–237 (1994). doi: 10.1002/gea.3340090303
58. B. H. Dahlin, in *Actes du XLII^e Congrès International des Américanistes*, vol. 8, pp. 305–312 (1979).
59. A. H. Siemens, D. E. Puleston, Ridged fields and associated features in southern Campeche: New perspectives on the Lowland Maya. *Am. Antiq.* **37**, 228–239 (1972). doi: 10.2307/278209
60. D. E. Puleston, in *Social Process in Maya Prehistory: Studies in Honour of Sir Eric Thompson*, N. Hammond, Ed. (Academic Press, 1977), pp. 449–467.
61. B. L. Turner II, Prehistoric intensive agriculture in the Mayan lowlands. *Science* **185**, 118–124 (1974). doi: 10.1126/science.185.4146.118; pmid: 17810497
62. B. L. Turner II, P. D. Harrison, Prehistoric raised-field agriculture in the Maya lowlands. *Science* **213**, 399–405 (1981). doi: 10.1126/science.213.4506.399; pmid: 17760172
63. B. L. Turner II, P. D. Harrison, Eds., *Pulltrouser Swamp: Ancient Maya Habitat, Agriculture, and Settlement in Northern Belize* (Univ. of Texas Press, 1983).
64. E. Lemonnier, B. Vannière, Agrarian features, farmsteads, and homesteads in the Río Bec nuclear zone, Mexico. *Anc. Mesoam.* **24**, 397–413 (2013). doi: 10.1017/S0956536113000242
65. P. D. Harrison, in *The Managed Mosaic: Ancient Maya Agriculture and Resource Use*, S. L. Fedick, Ed. (Univ. of Utah Press, 1996), pp. 177–190.
66. M. D. Pohl *et al*., Early agriculture in the Maya Lowlands. *Lat. Am. Antiq.* **7**, 355–372 (1996). doi: 10.2307/972264
67. J. S. Jacob, Ancient Maya wetland agricultural fields in Cobweb Swamp, Belize: Construction, chronology, and function. *J. Field Archaeol.* **22**, 175–190 (1995).
68. M. D. Pohl, in *Ancient Maya Wetland Agriculture*, M. D. Pohl, Ed. (Waveland, Boulder, CO, 1990), pp. 1–20.
69. S. L. Fedick, A. Ford, The prehistoric agricultural landscape of the central Maya Lowlands: An examination of local variability in a regional context. *World Archaeol.* **22**, 18–33 (1990). doi: 10.1080/00438243.1990.9980126
70. P. D. Harrison, in *Pre-Hispanic Maya Agriculture*, P. D. Harrison, B. L. Turner II, Eds. (Univ. of New Mexico Press, 1978), pp. 247–253.
71. N. P. Dunning *et al*., Temple mountains, sacred lakes, and fertile fields: Ancient Maya landscapes in northwestern Belize. *Antiquity* **73**, 650–660 (1999). doi: 10.1017/S0003598X0006525X
72. S. Kepecs, S. Boucher, in *The Man-aged Mosaic: Ancient Maya Agriculture and Resource Use*, S. L. Fedick, Ed. (Univ. of Utah Press, 1996), pp. 69–91.
73. K. J. Johnston, The intensification of pre-industrial cereal agriculture in the tropics: Boserup, cultivation lengthening, and the Classic Maya. *J. Anthropol. Archaeol.* **22**, 126–161 (2003). doi: 10.1016/S0278-4165(03)00013-8
74. A. S. Z. Chase, J. Weishampel, Using LiDAR and GIS to investigate water and soil management in the agricultural terracing at Caracol, Belize. *Adv. Archaeol. Pract.* **4**, 357–370 (2016). doi: 10.7183/2326-3768.4.3.357
75. U. M. Cowgill, Soil fertility, population, and the ancient Maya. *Proc. Natl. Acad. Sci. U.S.A.* **46**, 1009–1011 (1960). doi: 10.1073/pnas.46.8.1009; pmid: 16590706
76. U. M. Cowgill, Soil fertility and the ancient Maya. *Trans. Conn. Acad. Arts Sci.* **42**, 1–56 (1961).
77. U. M. Cowgill, An agricultural study of the southern Maya Lowlands. *Am. Anthropol.* **64**, 273–286 (1962). doi: 10.1525/aa.1962.64.2.02a00030
78. R. E. Griffin, thesis, Pennsylvania State University (2012).
79. N. B. Schwartz, A note on 'weights, measures' and swidden. *Cult. Agric.* **27**, 9–12 (1985).
80. N. B. Schwartz, A. R. Corzo M, Swidden counts: A Petén, Guatemala, milpa system: production, carrying capacity, and sustainability in the southern Maya Lowlands. *J. Anthropol. Res.* **71**, 69–93 (2015). doi: 10.3998/jar.0521004.0071.104
81. J. D. Nations, R. B. Nigh, The evolutionary potential of Lacandon Maya sustained-yield tropical forest agriculture. *J. Anthropol. Res.* **36**, 1–30 (1980). doi: 10.1086/jar.36.1.3629550
82. A. Ford, K. C. Clarke, S. Morlet, Calculating Late Classic Lowland Maya population for the upper Belize River area. *Res. Rep. Belizean Archaeol.* **8**, 75–87 (2011).
83. A. Ford, R. Nigh, Origins of the Maya forest garden: Maya resource management. *J. Ethnobiol.* **29**, 213–236 (2009). doi: 10.2993/0278-0771-29.2.213
84. W. A. Haviland, Tikal, Guatemala, and Mesoamerican urbanism. *World Archaeol.* **2**, 186–197 (1970). doi: 10.1080/00438243.1970.9979473
85. W. A. Ashmore, Ed., *Lowland Maya Settlement Patterns* (Univ. of New Mexico Press, 1981).
86. T. P. Culbert, D. S. Rice, Eds., *Precolumbian Population History in the Maya Lowlands* (Univ. of New Mexico Press, 1990).
87. D. E. Puleston, *The Settlement of Survey of Tikal* (University Museum, Univ. of Pennsylvania, 1983).
88. A. Ford, *Population Growth and Social Complexity: An Examination of Settlement and Environment in the Central Maya Lowlands* (Arizona State University, 1986).
89. D. L. Webster, W. T. Sanders, P. van Rossum, A simulation of Copán population history and its implications. *Anc. Mesoam.* **3**, 185–197 (1992). doi: 10.1017/S095653610000239X
90. D. Simon, Urban environments: Issues on the peri-urban fringe. *Annu. Rev. Environ. Resour.* **33**, 167–185 (2008). doi: 10.1146/annurev.environ.33.021407.093240
91. W. R. Bullard Jr., Maya settlement pattern in northeastern Peten, Guatemala. *Am. Antiq.* **25**, 355–372 (1960). doi: 10.2307/277519
92. W. A. Haviland, in *Lowland Maya Settlement Patterns*, W. A. Ashmore, Ed. (Univ. of New Mexico Press, 1981), pp. 89–120.
93. A. F. Chase, D. Z. Chase, in *Perspectives on Ancient Maya Rural Complexity*, G. Iannone, S. V. Connell, Eds. (Cotsen Institute of Archaeology, Los Angeles, 2003), pp. 108–118.
94. S. R. Hutson, *The Ancient Urban Maya: Neighborhoods, Inequality, and Built Form* (Univ. Press of Florida, 2016).
95. D. B. Marken, in *Classic Maya Polities of the Southern Lowlands: Integration, Interaction, Dissolution*, D. B. Marken, J. L. Fitzsimmons, Eds. (Univ. Press of Colorado, 2015), pp. 123–166.
96. J. P. Baron, thesis, University of Pennsylvania (2013).
97. T. Barrientos Q., M. A. Canuto, D. Stuart, L. Auld-Thomas, M. Lamoureux-St-Hilaire, in *XXIX Simposio de Investigaciones Arqueológicas en Guatemala*, B. Arroyo, L. Méndez Salinas, L. Paiz, Eds. (Ministerio de Cultura y Deportes, Instituto de Antropología e Historia, Asociación Tikal, Guatemala, 2016), pp. 1–23.
98. M. A. Canuto, T. Barrientos Q., in *La Corona Notes* (2013); www.mesoweb.com/LaCorona/LaCoronaNotes01.pdf.
99. M. A. Canuto, T. Barrientos Q., in *XXXI Simposio de Investigaciones Arqueológicas en Guatemala*, B. Arroyo, L. Méndez Salinas, L. Paiz, Eds. (Ministerio de Cultura y Deportes, Instituto de Antropología e Historia, Asociación Tikal, Guatemala, 2018), pp. 303–314.
100. S. Martin, "Wives and Daughters on the Dallas Altar." *Mesoweb* (2008); www.mesoweb.com/articles/Martin/Wives&Daughters.pdf.
101. D. Stuart *et al*., in *XXVII Simposio de Investigaciones Arqueológicas en Guatemala*, B. Arroyo, L. Méndez Salinas, A. Rojas, Eds. (Ministerio de Cultura y Deportes, Instituto de Antropología e Historia, Asociación Tikal, Guatemala, 2014), pp. 435–448.
102. M. A. Canuto, T. Barrientos Q., La Corona: Un acercamiento a las políticas del reino Kaan desde un centro secundario del noroeste de Petén. *Estud. Cult. Maya* **XXXVIII**, 14–43 (2011).
103. V. L. Scarborough, Ecology and ritual: Water management and the Maya. *Lat. Am. Antiq.* **9**, 135–159 (1998). doi: 10.2307/971991
104. A. S. Z. Chase, Beyond elite control: Residential reservoirs at Caracol, Belize. *Wiley Interdiscipl. Rev. Water* **3**, 885–897 (2016). doi: 10.1002/wat2.1171
105. E. Akpinar-Ferrand, N. P. Dunning, D. L. Lentz, J. G. Jones, Use of aguadas as water management sources in two southern Maya Lowland sites. *Anc. Mesoam.* **23**, 85–101 (2012). doi: 10.1017/S0956536112000065
106. J. L. Brewer, Householders as water managers: A comparison of domestic-scale water managment practices from two central Maya Lowland sites. *Anc. Mesoam.* **29**, 197–217 (2018). doi: 10.1017/S0956536117000244
107. K. L. Davis-Salazar, Late Classic Maya water management and community organization at Copan, Honduras. *Lat. Am. Antiq.* **14**, 275–299 (2003). doi: 10.2307/3557561
108. K. J. Johnston, Lowland Maya water management practices: The household exploitation of rural wells. *Geoarchaeology* **19**, 265–292 (2004). doi: 10.1002/gea.10117
109. V. L. Scarborough, in *Economic Aspects of Water Management in the Prehispanic New World*, V. L. Scarborough, B. L. Isaac, Eds. (JAI Press, 1993), pp. 17–69.
110. E. Weiss-Krejci, T. Sabbas, The potential role of small depressions as water storage features in the central Maya Lowlands. *Lat. Am. Antiq.* **13**, 343–357 (2002). doi: 10.2307/972115
111. V. L. Scarborough *et al*., Water and sustainable land use at the ancient tropical city of Tikal, Guatemala. *Proc. Natl. Acad. Sci. U.S.A.* **109**, 12408–12413 (2012). doi: 10.1073/pnas.1202881109; pmid: 22802627
112. V. L. Scarborough, in *Managed Mosaic: Ancient Maya Agriculture and Resource Use*, S. L. Fedick, Ed. (Univ. of Utah Press, 1996), pp. 304–314.
113. J. Kantner, in *Movement, Connectivity, and Landscape Change in the Ancient Southwest: The 20th Anniversary Southwest Symposium*, M. C. Nelson, C. Strawhacker, Eds. (Univ. Press of Colorado, 2011), pp. 363–374.
114. I. Graham, *Archaeological Explorations in El Peten, Guatemala* (Middle American Research Institute, Tulane University, 1967).
115. R. D. Hansen, in *Function and Meaning in Classic Maya Architecture*, S. D. Houston, Ed. (Dumbarton Oaks Research Library and Collection, Washington, DC, 1998), pp. 49–122.
116. E. Hernández, T. Schreiner, C. Morales Aguilar, in *XXVI Simposio de Investigaciones Arqueológicas en Guatemala*, B. Arroyo, L. Méndez Salinas, Eds. (Museo Nacional de Arqueología y Etnología, Guatemala, 2013), pp. 939–950.
117. J. M. Shaw, Maya *sacbeob*: Form and function. *Anc. Mesoam.* **12**, 261–272 (2001). doi: 10.1017/S0956536101121048
118. D. E. Puleston, D. W. Callender Jr., Defensive earthworks at Tikal. *Expedition* **9**, 40–48 (1967).
119. D. Webster *et al*., The great Tikal earthwork revisited. *J. Field Archaeol.* **32**, 41–64 (2007). doi: 10.1179/009346907791071700
120. D. L. Webster, in *Archaeological Investigations on the Yucatan Peninsula*, M. A. L. Harrison, R. Wauchope, Eds. (Tulane University, 1975), pp. 123–127.
121. D. Stuart, in *Mesoamerica's Classic Heritage: From Teotihuacan to the Aztecs*, D. Carrasco, L. Jones, S. Sessions, Eds. (Univ. Press of Colorado, 2000), pp. 465–514.
122. A. F. Chase, D. Z. Chase, J. F. Weishampel, Lasers in the jungle. *Archaeology* **63**, 27–29 (2010).

ACKNOWLEDGMENTS

The Pacunam LiDAR Initiative (PLI) was made possible because of planning, funding, and management by the Fundación Patrimonio Cultural y Natural Maya-PACUNAM. PLI's technology provider for the collection and processing of the 2016 lidar dataset was the NSF National Center for Airborne Laser Mapping (NCALM). Permissions for lidar collection and field work were granted to NCALM-Pacunam and participating archaeological projects by the Guatemalan Ministry of Culture and Sports of Guatemala. We thank three anonymous reviewers for their careful reading and helpful comments on earlier drafts of the manuscript. **Funding:** Supported by the Fundación Patrimonio Cultural y Natural Maya-PACUNAM through contributions from the Hitz Foundation and Pacunam's Guatemalan members (Cervecería Centro Americana, Grupo Campollo, Cementos Progreso, Blue Oil, Asociación de Azucareros de Guatemala-ASAZGUA, Grupo Occidente, Banco Industrial, Walmart Guatemala, Citi, Samsung, Disagro, Cofiño Stahl, Claro, CEG, Agroamerica, and Fundación Pantaleón). Additional funding for related fieldwork and data processing was provided by the Middle American Research Institute at Tulane University, Alphawood Foundation, Louisiana Board of Regents, CNRS, LabEx DynamiTe, the Slovak Research and Development Agency APVV-0864-12, and Scientific Grant Agency VEGA 1/0858/17. **Author contributions:** M.A.C., F.E.-B., and T.G.G. contributed to the planning of the research; M.A.C., F.E.-B., T.G.G., M.J.A., M.K., D.M., P.N., and R.S. supervised the work; J.C.F.-D. collected and processed the lidar data; M.A.C., F.E.-B., T.G.G., D.M., P.N., L.A.-T., C.C., D.C., C.R.C., T.D., T.L., A.T., and A.V. performed the analyses of the lidar data; M.A.C., F.E.-B., T.G.G., S.D.H., L.A.-T., and J.C.F.-D. drafted the manuscript; and M.A.C., F.E.-B., T.G.G., L.A.-T., and T.L. designed the figures. All authors discussed the results and commented on the manuscript. **Competing interests:** Authors declare no competing interests. **Data and materials availability:** Summary data are available in the tables included in the main text or the supplementary materials. Files containing the data derived from the lidar analyses used in this paper are available for download from http://doi:10.5061/dryad.k51j708.

SUPPLEMENTARY MATERIALS

www.sciencemag.org/content/361/6409/eaau0137/suppl/DC1
Materials and Methods
Supplementary Text
Figs. S1 and S2
Tables S1 to S4
References (*123*–*144*)

10.1126/science.aau0137

Science

Ancient lowland Maya complexity as revealed by airborne laser scanning of northern Guatemala

Marcello A. Canuto, Francisco Estrada-Belli, Thomas G. Garrison, Stephen D. Houston, Mary Jane Acuña, Milan Kovác, Damien Marken, Philippe Nondédéo, Luke Auld-Thomas, Cyril Castanet, David Chatelain, Carlos R. Chiriboga, Tomás Drápela, Tibor Lieskovský, Alexandre Tokovinine, Antolín Velasquez, Juan C. Fernández-Díaz and Ramesh Shrestha

Science **361** (6409), eaau0137.
DOI: 10.1126/science.aau0137

Classic Maya civilization in detail

Lidar (a type of airborne laser scanning) provides a powerful technique for three-dimensional mapping of topographic features. It is proving to be a valuable tool in archaeology, particularly where the remains of structures may be hidden beneath forest canopies. Canuto *et al.* present lidar data covering more than 2000 square kilometers of lowland Guatemala, which encompasses ancient settlements of the Classic Maya civilization (see the Perspective by Ford and Horn). The data yielded population estimates, measures of agricultural intensification, and evidence of investment in landscape-transforming infrastructure. The findings indicate that this Lowland Maya society was a regionally interconnected network of densely populated and defended cities, which were sustained by an array of agricultural practices that optimized land productivity and the interactions between rural and urban communities.

Science, this issue p. eaau0137; see also p. 1313